Binary Couette Flow with Hydrogen Injection into Carbon Dioxide and Nitrogen Streams

by

H. A. Simon

C. S. Liu

J. P. Hartnett

C. L. Chang

June 1964

National Aeronautics and Space Administration

Grant NSG 356

NOMENCLATURE

a	Speed of sound.
C_p	Constant pressure specific heat.
C_f	Skin friction coefficient.
D_{12}	Ordinary binary diffusion coefficient.
E	Eckert number = $M_e^2 (\gamma_e - 1)/(1 - T_w/T_e)$.
k	Thermal conductivity.
M	Mach number = u_e/a_e
Pr	Prandtl number = $\mu C_p/k$.
q	Heat transfer rate.
r	Recovery factor = $(T_r - T_e)/(u_e^2/2C_{p_e})$.
R	Universal gas constant.
Re_v	Reynolds number = $\rho v r_\delta$.
Sc	Schmidt number = $\mu/\rho D_{12}$.
T	Temperature.
u	x component of velocity.
U	Dimensionless velocity = u/u_e.
v	y component of velocity.
X	Mole fraction.
x	Coordinate parallel to plates.
y	Coordinate normal to plates.
Y	Mass fraction of injected gas.
γ	Specific heat ratio.
δ	Distance between plates.
η	Dimensionless coordinate = r/r_δ.
r	Transformed coordinate = $\int_0^y dy/\mu$.
θ	Dimensionless temperature = $(T - T_w)/(T_e - T_w)$.

μ Dynamic viscosity.

ν Kinematic viscosity.

ρ Mass density.

Subscripts

1 Injected gas.

2 Main stream gas.

w At stationary plate.

e At moving plate.

o Without blowing.

r Recovery or adiabatic wall condition.

TABLE OF CONTENTS

Binary Couette Flow with Hydrogen Injected into Carbon Dioxide and Nitrogen Streams

1.0 INTRODUCTION

Considerable interest has been focussed on mass transfer cooling as a means for protecting re-entering vehicles against frictional heating. The problem is a complex one, as in general, the most suitable coolant gas is different from that of the free stream, so that binary boundary layers have to be considered. Further, at the large temperature differences encountered, the gases display considerable property variations, and may also undergo dissociation and ionization. Ref. 1 contains a review of some of the approaches that have been used on this problem. In all cases air has been considered as the main stream gas, and an effort has been made to obtain engineering correlations for different coolant gases.

The present report is concerned with the injection of Hydrogen into free stream gases other than air, viz. Nitrogen or Carbon Dioxide. This study has been stimulated by the possibility of visiting neighboring planets where a variety of different atmospheres may be encountered. However, more mundane applications can be envisaged where surfaces require thermal protection from high temperature environments other than air.

Any simplification that can be used without concealing the most important aspects of the actual conditions is of value. Thus in the first instance this study uses the one-dimensional Couette flow model to simulate the two-dimensional, laminar, boundary layer. Variable properties have been included, though

not to the extent of allowing for dissociation and ionization. In the Couette flow model the velocity of the moving plate represents the free stream velocity, while the distance between the plates simulates the boundary layer thickness. A later phase of this present work will compare the Couette flow results with those for the two-dimensional laminar boundary layer using the same gases, so that the value of the Couette flow model as a basis for design information may be assessed.

To reduce the bulk of the present report only a few typical curves have been submitted. The full set of results in graphical or numerical form are available if required.

2.0 ANALYSIS

Figure 1, shows the Couette flow model. The lower porous plate, at y = 0, is held stationary, while the upper porous plate, at y = δ, moves in its own plane in the positive x direction with a uniform velocity u_e. The lower plate is at the temperature T_w and the upper plate at T_e. A coolant gas, initially at the temperature T_w, is introduced perpendicularly into the flow through the stationary plate, and removed through the upper plate.

2.1 Assumptions

The following assumptions have been made:

a) The model is one dimensional.

b) The flow is steady.

c) Both plates are impermeable to the main stream gas.

d) Gas properties depend on local mixture concentration and temperature.

e) Radiation heat transfer is neglected.

f) Thermal diffusion effects are neglected.

2.2 Basic Equations

In the light of the above assumptions, the following differential equations govern the flow.

Continuity equation.

$$\frac{d(\rho v)}{dy} = 0 \qquad (2.1.1)$$

Momentum equation.

$$\rho v \frac{du}{dy} = \frac{d}{dy}\left(\mu \frac{du}{dy}\right) \qquad (2.1.2)$$

Energy equation.

$$\rho v C_p \frac{dT}{dy} = \frac{d}{dy}\left(k \frac{dT}{dy}\right) + \mu \left(\frac{du}{dy}\right)^2 + \rho D_{12} \left(C_{p_1} - C_{p_2}\right) \frac{dY}{dy} \cdot \frac{dT}{dy} \qquad (2.1.3)$$

Species equation.

$$\rho v \frac{dY}{dy} = \frac{d}{dy}\left(\rho D_{12} \frac{dY}{dy}\right) \qquad (2.1.4)$$

The boundary conditions are:

At $y = 0$

$$u = 0$$

$$T = T_w$$

$$Y = Y_w$$

At $y = \delta$

$$u = u_e$$

$$T = T_e$$

$$Y = Y_e$$

From (2.1.1)

$$\rho v = (\rho v)_w = \text{constant} \qquad (2.1.5)$$

As the stationary wall is impermeable to the main stream gas

$$(\rho v)_w (1 - Y_w) = -\left(\rho D_{12} \frac{dY}{dy}\right)_w \qquad (2.1.6)$$

Integrating (2.1.4) with the aid of (2.1.5), and combining with (2.1.6) gives

$$\rho v (1 - Y) = -\rho D_{12} \frac{dY}{dy} \qquad (2.1.7)$$

This implies that all planes parallel to the walls are impermeable to the main stream gas, a result which follows directly from the assumption of one-dimensional flow.

The perfect gas law is employed to calculate the specific heat of the gas mixture.

$$C_p = C_{p_1} Y + (1 - Y) C_{p_2} \tag{2.1.8}$$

Equations (2.1.7) and (2.1.8) combined with the energy equation (2.1.3) give,

$$\rho v C_{p_1} \frac{dT}{dy} = \frac{d}{dy} \left(k \frac{dT}{dy}\right) + \mu \left(\frac{du}{dy}\right)^2 \tag{2.1.9}$$

This form of the energy equation contains the specific heat of the coolant gas only, due to the fact that all planes parallel to the walls are impermeable to the main stream gas, the coolant gas alone moving from one temperature level to another.

2.3 Dimensionless Form of Equations

Introduce the following new variables:

$$\eta = \int_o^y \frac{dy}{\mu}$$

$$\zeta = \eta/\eta_\delta \qquad \text{where } \eta_\delta = \int_o^\delta \frac{dy}{\mu}$$

$$U = u/u_e$$

$$\theta = \frac{T - T_w}{T_e - T_w}$$

The basic equations in dimensionless form are:

Momentum equation

$$Re_v \frac{dU}{d\zeta} = \frac{d^2U}{d\zeta^2} \tag{2.3.1}$$

Energy equation

$$Re_v \Phi C_p \frac{d\theta}{d\zeta} = \frac{d}{d\zeta} \left(\frac{1}{\Phi_{Pr}} \frac{d\theta}{d\zeta}\right) + E \left(\frac{dU}{d\zeta}\right)^2 \tag{2.3.2}$$

Species equation

$$Re_v \, Sc \, (1 - Y) = - \frac{dY}{d\zeta} \qquad (2.3.3)$$

Where

$$Re_v = \rho v \tau_\delta$$

$$E = \frac{M_e^2 \, (\gamma_e - 1)}{(1 - T_w / T_e)}$$

$$M_e = u_e / a_e$$

$$a_e^2 = \gamma_e R T_e = C_{p_e} \, (\gamma_e - 1) \, T_e$$

$$\Phi_{C_p} = C_{p_l} / C_{p_e}$$

$$\Phi_{Pr} = \mu C_{p_e} / k$$

$$Sc = \mu / \rho D_{12}$$

and the boundary conditions are:

At $\zeta = 0$

$$U = 0$$

$$\theta = 0$$

$$Y = Y_w$$

At $\zeta = 1$

$$U = 1$$

$$\theta = 1$$

$$Y = Y_e$$

The transformation used uncouples the momentum and energy equations, simplifying the computation considerably.

Notice that as the species equation is of first order, only one of the values Y_w and Y_e may be prescribed. In the analysis Y_e is chosen to be negligibly small in an effort to

simulate the two-dimensional laminar boundary layer. This introduces a note of unreality as it follows that the transverse velocity becomes very large at the moving plate.

With Y_e prescribed, equation (2.3.3) gives Y_w as,

$$Y_w = 1 - (1 - Y_e) \exp \left(-Re_v \int_o^1 Sc \, d\zeta\right) \qquad (2.3.4)$$

The solution of the momentum equation is

$$U = \frac{[\exp (Re_v \zeta)] - 1}{[\exp (Re_v)] - 1} \qquad (2.3.5)$$

The energy equation may now be written

$$Re_v \, \Phi_{C_p} \frac{d\theta}{d\zeta} = \frac{d}{d\zeta} \left(\frac{1}{\Phi_{Pr}} \frac{d\theta}{d\zeta}\right) + B_o \exp (2 Re_v \zeta)$$

where

$$B_o = \frac{E \, Re_v^2}{[\exp (Re_v) - 1]^2}$$

By integration,

$$\frac{d\theta}{d\zeta} = \left[-B_o \int_o^\zeta \exp \left(2Re_v\zeta - \int_o^\zeta \Phi_{Pr} \, \Phi_{C_p} \, Re_v \, d\zeta\right) d\zeta + C_1\right] \left[\Phi_{Pr} \exp \left(\int_o^\zeta \Phi_{Pr} \, \Phi_{C_p} \, Re_v \, d\zeta\right)\right] \qquad (2.3.6)$$

$$\theta = \int_o^\zeta \left\{ \left[-B_o \int_o^\zeta \exp \left(2Re_v \, \zeta - \int_o^\zeta \Phi_{Pr} \, \Phi_{C_p} \, Re_v \, d\zeta\right) d\zeta + C_1\right] \left[\Phi_{Pr} \exp \left(\int_o^\zeta \Phi_{Pr} \, \Phi_{C_p} \, Re_v \, d\zeta\right)\right] \right\} d\zeta \qquad (2.3.7)$$

where

$$C_1 = \frac{1 + B_o \int_o^1 \Phi_{Pr} \, F_1 (\zeta) \left\{ \int_o^\zeta [\exp (2Re_v \, \zeta)/F_1 (\zeta)] \, d\zeta \right\} d\zeta}{\int_o^1 \Phi_{Pr} \, F_1 (\zeta) \, d\zeta}$$

$$F_1(\zeta) = \exp\left[\int_0^{\zeta} \phi_{Pr}\, \phi_{C_p}\, Re_v\, d\zeta\right]$$

The solution of the species equation is given by.

$$Y = 1 - (1 - Y_e) \exp\left(-\int_{\zeta}^{1} Re_v\, Sc\, d\zeta\right) \qquad (2.3.8)$$

2.4 Solid Wall Case

In the solid wall case, the mass transfer through the porous plates is zero, so that

$$\rho v = 0$$

The differential equations now reduce to

$$\frac{d}{dy}\left(\mu \frac{du}{dy}\right) = 0 \qquad (2.4.1)$$

$$\frac{d}{dy}\left(k \frac{dT}{dy}\right) + \mu\left(\frac{du}{dy}\right)^2 = 0 \qquad (2.4.2)$$

The solutions to these equations are

$$U = \zeta \qquad (2.4.3)$$

$$\theta = -E \int_0^{\zeta} \phi_{Pr}\, \zeta\, d\zeta + B_1 \int_0^{\zeta} \phi_{Pr}\, d\zeta \qquad (2.4.4)$$

where

$$B_1 = \frac{1 + E\int_0^1 \phi_{Pr}\, \zeta d\zeta}{\int_0^1 \phi_{Pr}\, d\zeta}$$

2.5 Skin Friction

The skin friction coefficient is defined as

$$C_f = \frac{\tau_w}{\frac{1}{2}\rho_e u_e^2} = \frac{\left(\mu \frac{du}{dy}\right)_w}{\frac{1}{2}\rho_e u_e^2} \qquad (2.5.1)$$

Upon transformation this becomes

$$C_f = \left(\frac{dU}{d\zeta}\right)_w \Big/ \frac{1}{2} \rho_e u_e \eta_\delta \tag{2.5.2}$$

where

$$\eta_\delta = \int_o^\delta \frac{dy}{\mu} = \delta \Big/ \int_o^1 \mu d\zeta$$

The ratio of the skin friction with blowing, to that with no blowing is given by

$$C_f/C_{f_o} = \left\{\left(\int_o^1 \mu d\zeta\right)_w \Big/ \left(\int_o^1 \mu d\zeta\right)_{w_o}\right\}\left(\frac{dU}{d\zeta}\right)_w \tag{2.5.3}$$

2.6 Heat Transfer

The heat transfer at the wall due to conduction is given by

$$q_w = \left(k \frac{dT}{dy}\right)_w \tag{2.6.1}$$

Upon transformation this becomes

$$q_w = \left\{\frac{k\,(T_e - T_w)}{\mu \eta_\delta} \frac{d\theta}{d\zeta}\right\}_w \tag{2.6.2}$$

The ratio of the heat transfer with blowing to that without blowing, is given by:

$$q_w/q_{w_o} = \frac{\left(\int_o^1 \mu d\zeta\right)\left(\frac{d\theta}{d\zeta}\right)_w \left(\frac{k}{\mu}\right)_w}{\left(\int_o^1 \mu d\zeta\right)_o \left(\frac{d\theta}{d\zeta}\right)_{w_o} \left(\frac{k}{\mu}\right)_{w_o}}$$

$$= \frac{\left[Pr^{-1} C_p \left(\frac{d\theta}{d\zeta}\right)\right]_w \left[\int_o^1 \mu d\zeta\right]}{\left[Pr^{-1} C_p \left(\frac{d\theta}{dy}\right)\right]_{w_o} \left[\int_o^1 \mu d\zeta\right]_o} \tag{2.6.3}$$

2.7 Recovery Factor

The adiabatic wall temperature T_r is defined as the temperature of the stationary wall when

$$\left(\frac{dT}{dy}\right)_w = 0$$

The recovery factor, r, is defined as

$$r = \frac{T_r - T_e}{u_e^2/2C_{p_e}} \qquad (2.7.1)$$

θ_r is obtained from equation (2.3.7) by putting $C_1 = 0$.

2.8 Computation

A straightforward iteration technique was used in calculating the temperature and concentration profiles. The gas properties were calculated as described in Appendix A.1. Linear profiles were assumed initially and applied to equations (2.3.7) and (2.3.8) in turn giving new Y and θ profiles. This procedure was continued until

$$\sum_{n=1}^{J} \frac{Y_{i+1}(n) - Y_i(n)}{J} < \epsilon$$

$$\sum_{n=1}^{J} \frac{\theta_{i+1}(n) - \theta_i(n)}{J} < \epsilon$$

where ϵ is arbitrarily chosen as 10^{-6}. Here i refers to the i^{th} iteration, and n denotes the n^{th} point in the boundary layer which is divided into J points.

The following values of the independent parameters were used in the computation:

$T_e = 213°K$ for all cases.

M_e = 4, 8, 12

T_w = 436, 872, 1308°K

Re_v = 0.0, 0.15, 0.30, 0.50, 1.0, 2.0, 3.0, 5.0

The pressure was taken as 1 atmosphere in all cases.

2.7 Recovery Factor

The adiabatic wall temperature T_r is defined as the temperature of the stationary wall when

$$\left(\frac{dT}{dy}\right)_w = 0$$

The recovery factor, r, is defined as

$$r = \frac{T_r - T_e}{u_e^2/2C_{p_e}} \qquad (2.7.1)$$

θ_r is obtained from equation (2.3.7) by putting $C_1 = 0$.

2.8 Computation

A straightforward iteration technique was used in calculating the temperature and concentration profiles. The gas properties were calculated as described in Appendix A.1. Linear profiles were assumed initially and applied to equations (2.3.7) and (2.3.8) in turn giving new Y and θ profiles. This procedure was continued until

$$\sum_{n=1}^{J} \frac{Y_{i+1}(n) - Y_i(n)}{J} < \epsilon$$

$$\sum_{n=1}^{J} \frac{\theta_{i+1}(n) - \theta_i(n)}{J} < \epsilon$$

where ϵ is arbitrarily chosen as 10^{-6}. Here i refers to the i^{th} iteration, and n denotes the n^{th} point in the boundary layer which is divided into J points.

The following values of the independent parameters were used in the computation:

$T_e = 213°K$ for all cases.

M_e = 4, 8, 12

T_w = 436, 872, 1308°K

Re_v = 0.0, 0.15, 0.30, 0.50, 1.0, 2.0, 3.0, 5.0

The pressure was taken as 1 atmosphere in all cases.

in Figs. 5, 6 and 7, and it is clear that for each binary mixture the profiles are almost identical at one value of the blowing parameter, regardless of the Mach number and wall temperature chosen. An examination of Fig. 8 indicates that the Schmidt number is a weak function of the temperature but strongly dependent on concentration. Thus for Y_e negligible in all cases, equation (2.3.8) shows that the concentration profile is primarily a function of Re_v.

3.3 Temperature Profiles

The temperature profiles are presented in Figs. 9 - 14

Clearly, increased blowing reduces the temperature gradient at the wall in most cases.

For a low Mach number (Me = 4) and a high wall temperature (T_w = 872 or 1308°K) the maximum temperature is that at the stationary wall. Here heat flows by conduction from the wall to the fluid.

At the higher Mach numbers the increased heat generation due to friction causes the maximum temperature to occur in the fluid. In such cases the stationary wall is being heated by conduction from the fluid. The effect of blowing is to reduce this maximum temperature and move it closer to the outer wall. Injecting gas at the wall temperature, reduces temperature differences near the stationary wall due to the thermal capacity of the injected gas. Furthermore, momentum effects, as indicated by the velocity profiles, move the region of greatest frictional dissipation closer to the moving wall as the blowing parameter Re_v increases.

Examination of the dimensionless temperature profiles can only reveal the direction of heat transfer by conduction.

The amount of heat transferred depends also upon the thermal conductivity of the binary mixture at the point considered. The direction of heat transfer may be inferred from the curves presented, as in all cases the moving wall temperature is less than that of the stationary wall; thus the gradient of θ and of T will be of the opposite sign.

3.4 Skin Friction

The skin friction depends on the product of the viscosity and the velocity gradient. Figs. 15 - 17 show that the skin friction at the stationary wall is decreased with blowing, as not only is the velocity gradient reduced there, but the injected gas, hydrogen, has a lower viscosity than either nitrogen or carbon dioxide at the same temperature. One exception to this occurs at M = 4 for the high wall temperature (1308°K) at low blowing rates, where $C_f/C_{f_o} > 1$. Fig. 11 indicates that under these conditions the temperature throughout the field is increased by blowing. Thus the reduction in the velocity gradient at the wall must be offset by an increase in the viscosity in this case.

3.5 Recovery Factor

The adiabatic wall temperature is defined as the temperature of the stationary wall when

$$\left(\frac{dT}{dy}\right)_w = 0$$

The recovery factor is defined by

$$r = \frac{T_r - T_e}{u_e^2/2c_{p_e}}$$

Fig. 18 obtained from the constant property analysis of Appendix A-2,

shows that the ratio r/r_o is reduced with blowing for Pr<1.0, and increased by blowing for Pr>1.0. Also $r/r_o = 1.0$ for Pr = 1.0.

Fig. 19 indicates that in the cases considered here, r/r_o generally increases with blowing, a surprising result as Pr<1.0 for all pure components and the binary mixtures involved. Notice, however, that the energy equation (2.1.9) contains the specific heat of the injected gas only, while all other properties are for the mixture. If expressed in dimensionless form, an effective Prandtl number $\frac{Cp_1 \mu}{k}$ which is in general greater than one, arises. In considering shear work and heat conduction, the values of μ and k for the mixture are applicable. However the Couette flow model is set up such that only the injected gas is convected from one layer to another, so that Cp_1 becomes the relevant specific heat.

3.6 Heat Transfer

As defined in equation (2.6.1) the heat transfer at the wall only includes that due to conduction. The enthalpy flow due to the secondary gas is not included.

The ratio given by equation (2.6.3) is shown in Figs. 20 - 25. As described in section (3.3), increased blowing reduces the temperature gradient at the wall in most cases, so that one might expect the heat transfer ratio, q_w/q_{w_o}, to decrease with increased blowing. This is the predominant effect, particularly at high values of the blowing parameter. However, it is clear from Figs. 20, 21 and 24 that other influences are present.

A second influence arises due to property variations. At low injection rates, for which the temperature gradient reduction

is still small, the presence of Hydrogen near the wall may increase the mixture thermal conductivity sufficiently for the heat transfer to increase. (See Fig. 21).

Finally, when the wall temperature is close to the recovery temperature, the heat transfer ratio may be expected to show violent variations. In Fig. 24 for $T_w = 1308°K$, q_w/q_{w_o} increases more than five-fold at low blowing rates. The corresponding recovery temperature is 1340°K for $Re_v = 0$. In such cases blowing may not reduce the temperature gradient at the wall, and in fact the shape of the recovery temperature variation displayed in Fig. 26 indicates that the influence on the temperature gradient need not be monotonic with increasing blowing. In the case cited, q_{w_o} is very small and a small amount of blowing increases the heat transfer ratio substantially.

In Fig. 20 for $T_w = 872°K$, the recovery temperature is 700°K and again q_{w_o} is small. Here the effect of blowing is to decrease the ratio sharply. In certain cases the heat transfer ratio may be expected to become negative, andeven to oscillate about zero. This would occur for $H_2:N_2$ with $T_w = 2300°K$ and $M = 8$, though this case was not considered here. This conclusion is again evident from an examination of Fig. 26.

3.7 The Couette Flow Model

The value of the Couette flow model for predicting results in the binary boundary layer can only be assessed when the boundary layer results are available. However it is clear that in certain respects the Couette flow model departs considerably from the actual conditions. The assumption of a negligible

concentration of the injected gas at the moving wall entails an extremely high value of the transverse velocity component at the moving wall to satisfy continuity. More serious, is the occurrence of an effective Prandtl number that is greater than one, as under actual conditions the Prandtl number will always be less than one for the components considered. The exclusion of the main stream gas from any participation with regard to convection may be expected to falsify the heat transfer and recovery temperature results as compared with the boundary layer. Clearly one of the main points of departure concerns the boundary conditions at the moving wall, though hopefully, this may not be too serious, as the conditions at the stationary wall are of paramount importance in predicting heat transfer and skin friction.

4.0 CONCLUSIONS

Calculations based on the Couette flow model for Hydrogen injection into a main stream gas of Nitrogen or Carbon Dioxide, predict substantial reductions in heat transfer and skin friction as the blowing parameter is increased. However, the heat transfer ratio q_w/q_{w_o} exhibits erratic behavior when the wall temperature is close to the recovery temperature.

Several departures from boundary layer behavior are observed, one of the most interesting, in judging the validity of the model, is the occurrence of an effective Prandtl number greater than one, with the corresponding influence on the recovery factor.

ACKNOWLEDGEMENT

Professor J. L. Novotny provided valuable guidance in the selection of the appropriate thermodynamic and transport properties and the authors acknowledge this assistance. In addition, appreciation is expressed to the staff of the Computing Center, University of Delaware for their cooperation in carrying out the numerical calculations.

Appendix A.1

Calculation of gas properties

The thermodynamic and transport properties of hydrogen-carbon-dioxide and hydrogen-nitrogen gas mixtures were calculated by the methods listed below. The gas mixtures were considered to be at atmospheric pressure while the temperature ranged from 100°K to 4050°K.

a. Density:

Compressibility factors for hydrogen, carbon dioxide, and nitrogen differ from unity by less than 0.5 percent at 300°K and less than 0.008 percent for higher temperature. (Ref. 2). Therefore, the perfect gas law may be employed for the determination of the density:

$$\rho = Mp/RT \qquad (A.1.1)$$

where:

ρ, density in gm/cm^3

M, molecular weight

p, pressure (1 atm)

R, universal gas constant,
$82.0618\ cm^3\ atm/°K gm\text{-}mole$

T, temperature in °K.

For gas mixtures the density is calculated by

$$\rho_{12} = p/\{[1/M_2 + (1/M_1 - 1/M_2)\ Y]\ RT\} \qquad (A.1.2)$$

where Y is mass fraction of the injected component and the subscripts 1 and 2 represent the injected and the free stream components of the mixture, respectively.

b. Specific Heat:

Ideal-gas constant pressure specific heat data (C_p/R) were taken from reference 2. Comparing these values with those given for the non-ideal gas in the same reference it is found that the deviation is very small.

The constant pressure specific heat of the gas mixtures was calculated as follows:

$$c_{p12} = Yc_{p1} + (1-Y)\, c_{p2} \qquad (A.1.3)$$

where c_p is the specific heat per gram and C_p is the constant pressure specific heat per mole.

The relationship between constant pressure specific heat and the constant volume specific heat can be expressed as:

$$C_p - C_v = R \qquad (A.1.4)$$

where R is universal gas constant, 1.98719 cal/°K/mole.

Equation (A.1.4) is valid when the specific heat is variable.

The specific heat ratio, $\gamma = c_p/c_v$, approaches unity at high temperature.

c. Viscosity:

The viscosity for the pure gases has been calculated by the method of reference 3 (p. 528).

$$\mu x 10^7 = 266.93 \frac{\sqrt{MT}}{\sigma^2\, \Omega(2,2)^*(T^*)} \qquad (A.1.5)$$

where:

μ, viscosity, gm/cm-sec (poise)

T, reduced temperature, $T/(\epsilon/k)$

σ, collision diameter in Å

ϵ/k, potential parameter in °K.

σ and ϵ/k are given in Table A.1.1.

TABLE A.1.1

	ϵ/k	σ	Reference
H_2	86.1	2.729	4
N_2	91.46	3.681	5
CO_2	195.2	3.941	6

$\Omega^{(2,2)*}$ (T^*) was taken from Table I-M in reference

Following Wilke (Ref. 7) the viscosity for gas mixtures is given by

$$\mu_{mix} = \sum_{i \neq j} \frac{\mu_i}{1 + \varphi_{ij} X_j/X_i} \qquad (A.1.6)$$

and for binary mixtures

$$\mu_{12} = \mu_1/(1 + \varphi_{12} X_2/X_1) + \mu_2/(1 + \varphi_{21} X_1/X_2)$$

or

$$\mu_{12} = \mu_1/[1 + \varphi_{12} M_1 (1-Y)/M_2 Y] + \mu_2/[1 + \varphi_{21} M_2 Y/M_1 (1-Y)] \qquad (A.1.7)$$

where:

X, mole fraction $(X_1/X_2 = M_2 Y_1/M_1 Y_2)$

φ_{ij} is given by

$$\varphi_{ij} = \frac{\left\{1 + (\mu_i/\mu_j)^{1/2} (M_j/M_i)^{1/4}\right\}^2}{(4/\sqrt{2}) [1 + (M_i/M_j)]^{1/2}} \qquad (A.1.8)$$

Examining the result from the calculation of equation (A.1.8) it is found that φ_{ij} is relatively independent of temperature. Values of φ_{ij} used are given Table A.1.2.

TABLE A.1.2

Mixture	$H_2 - CO_2$	$H_2 - N_2$
φ_{12}	2.220	1.894
φ_{21}	0.2019	0.2766

In order to check the validity of Table A.1.2, a comparision between the viscosity calculated by using eq. (A.1.8) for φ_{ij} and the viscosity calculated by using Table A.1.2 for φ_{ij} has been made and the results show a maximum deviation of 0.3 percent for temperatures below 300°K for the $H_2 - CO_2$ mixture. The agreement is better than 0.2 percent for temperatures higher than 300°K for the $H_2 - CO_2$ mixture and for the whole temperature range considered for the $H_2 - N_2$ mixture.

d. Thermal Conductivity:

From reference 3 (p. 301) the thermal conductivity for a pure gas is given by

$$k = [(15 - 6\rho D/\mu)\,\gamma - (15 - 10\rho D/\mu)]\, c_v \mu/4 \qquad (A.1.9)$$

where:

c_v, constant volume specific heat

γ, ratio of specific heats = c_p/c_v.

Employing the definition of the gas constant,

$$R/M = c_p - c_v$$

$$k = [15/4 + (\rho D/\mu)\,(c_p M/R - 5/2)]\, \mu R/M.$$

$\mu/\rho D$ is the Schmidt number. A calculation has been performed to calculate the Schmidt number for H_2, CO_2, and N_2 (where D is the ordinary self-diffusion coefficient). It is found that the values lie between 0.75 and 0.76.

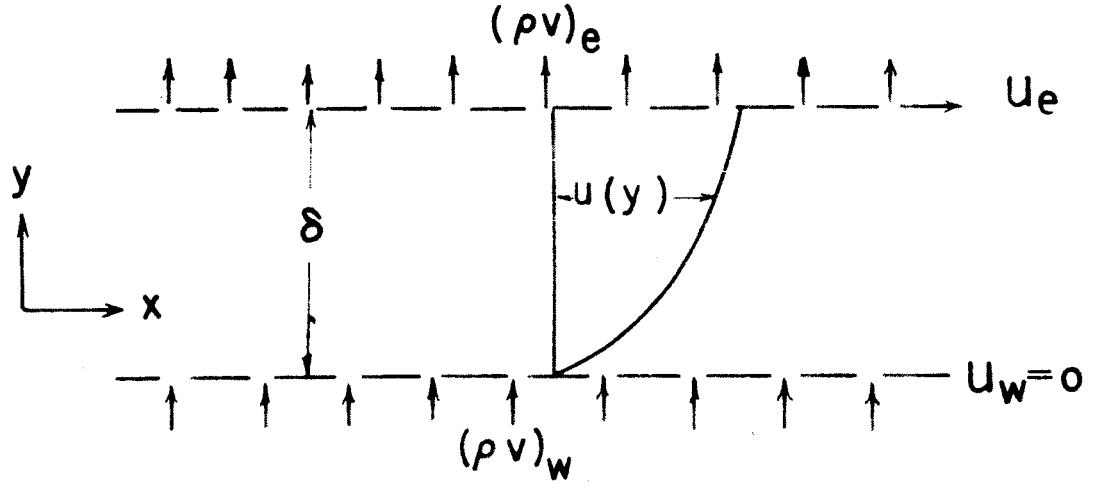

Fig. 1

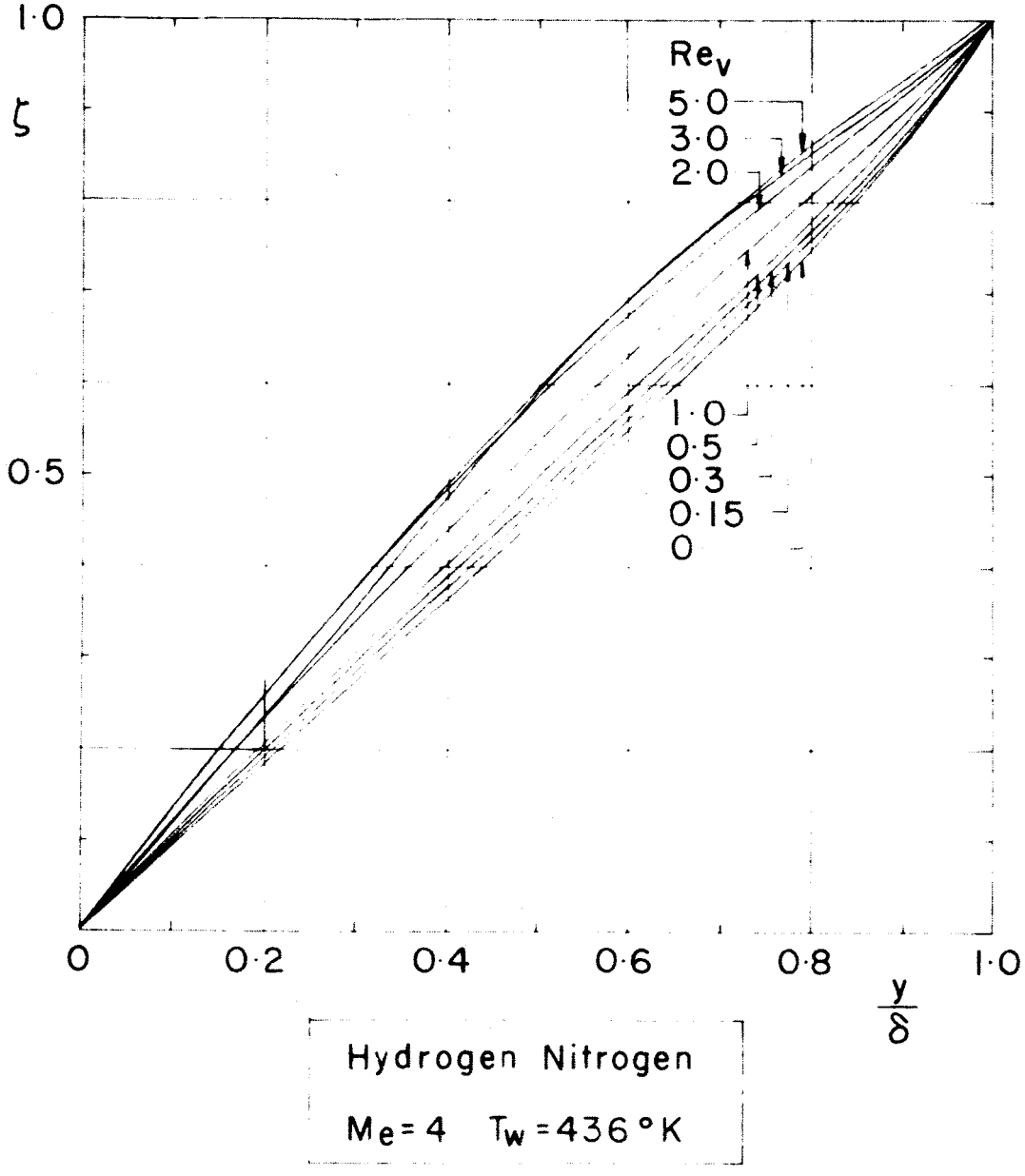
1·0
ζ
0·5
Re_v
5·0
3·0
2·0
1·0
0·5
0·3
0·15
0
0
0·2
0·4
0·6
0·8
1·0
y/δ
Hydrogen Nitrogen
Me = 4 Tw = 436 °K

Fig. 2

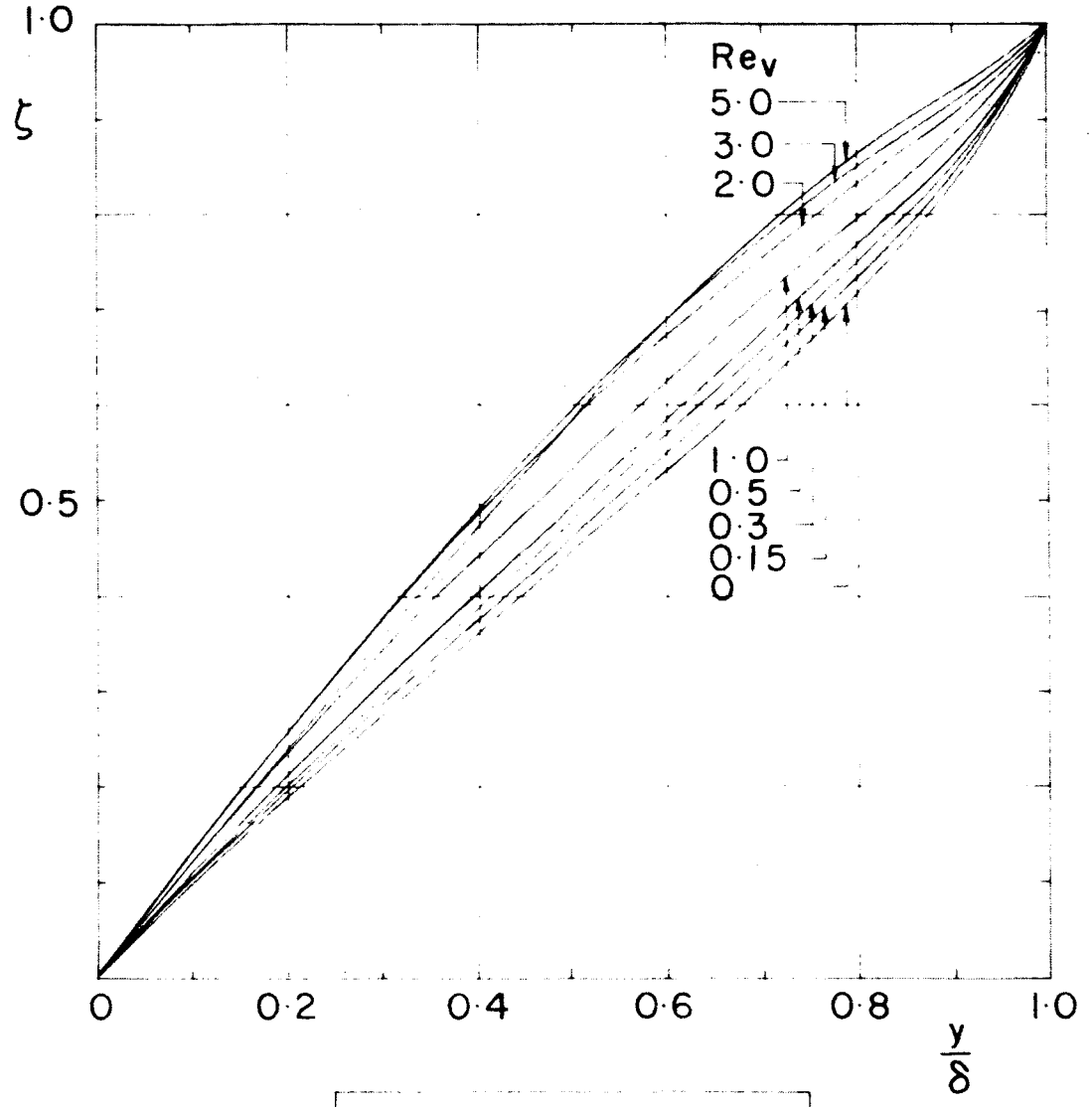
1·0
ζ
0·5
Re_v
5·0
3·0
2·0
1·0
0·5
0·3
0·15
0
0
0·2
0·4
0·6
0·8
1·0
y/δ
Hydrogen Nitrogen
M_e = 12 T_w = 1308°K

Fig. 3

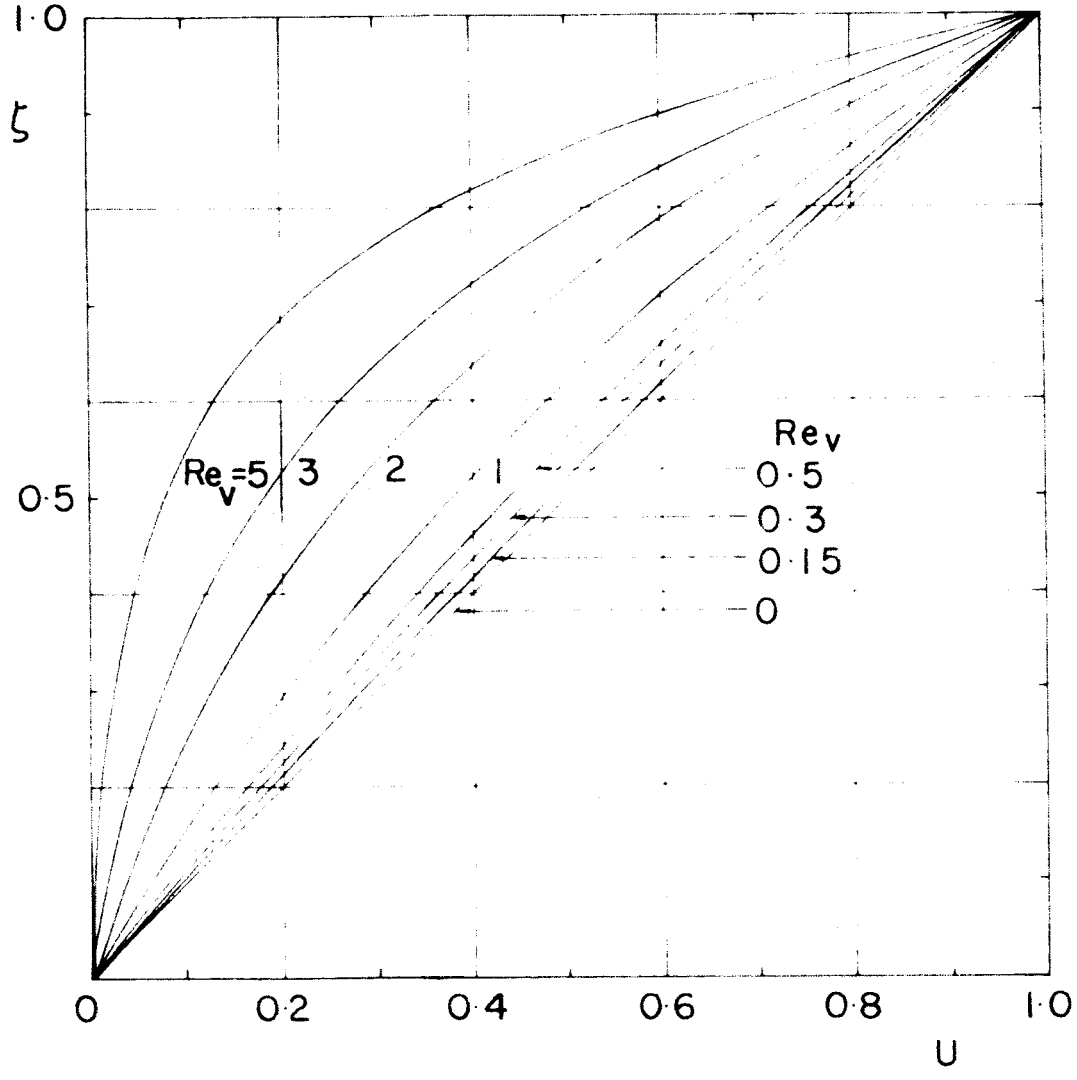

Fig. 4

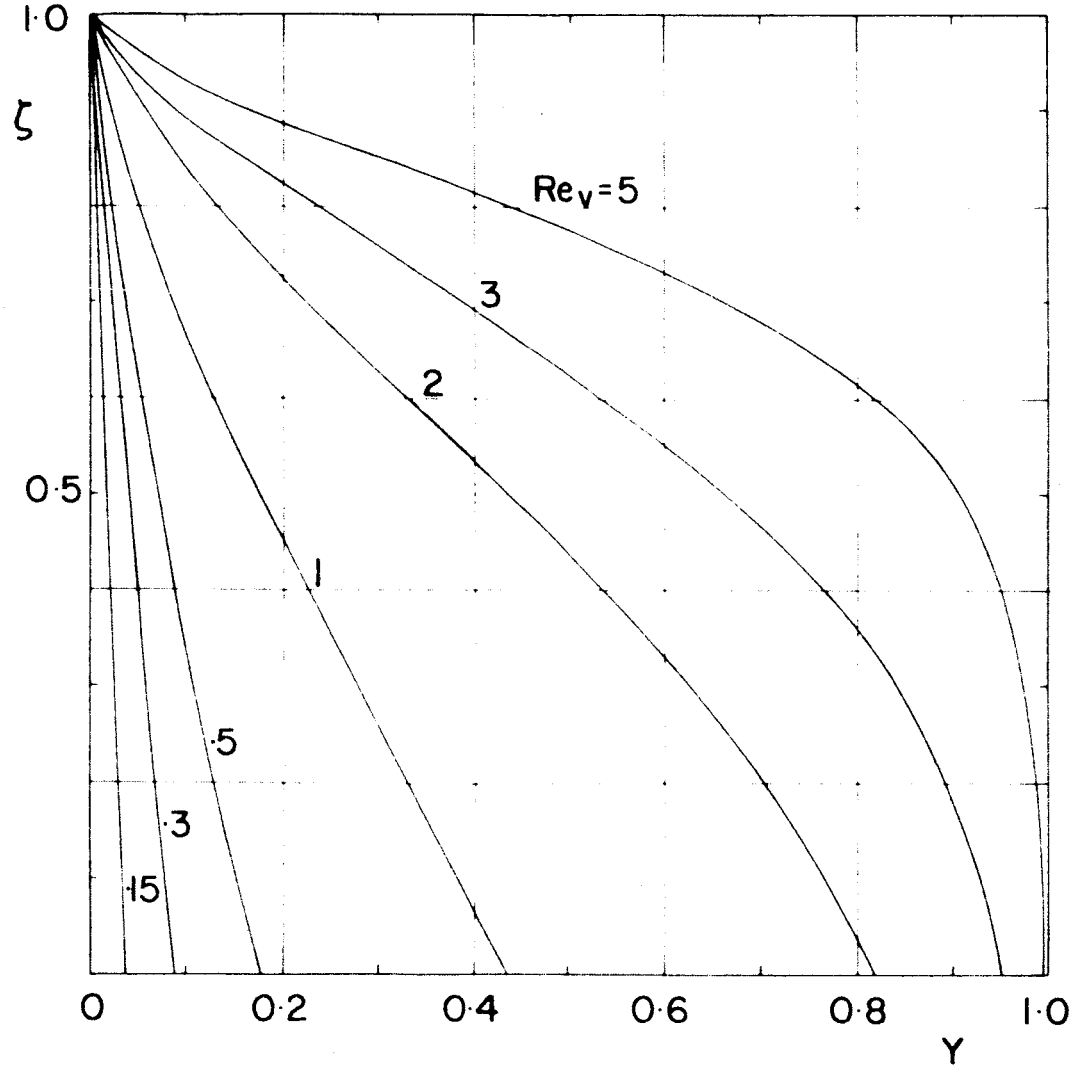

Hydrogen	Nitrogen
$M_e = 4$	$T_w = 436°K$

Fig. 5

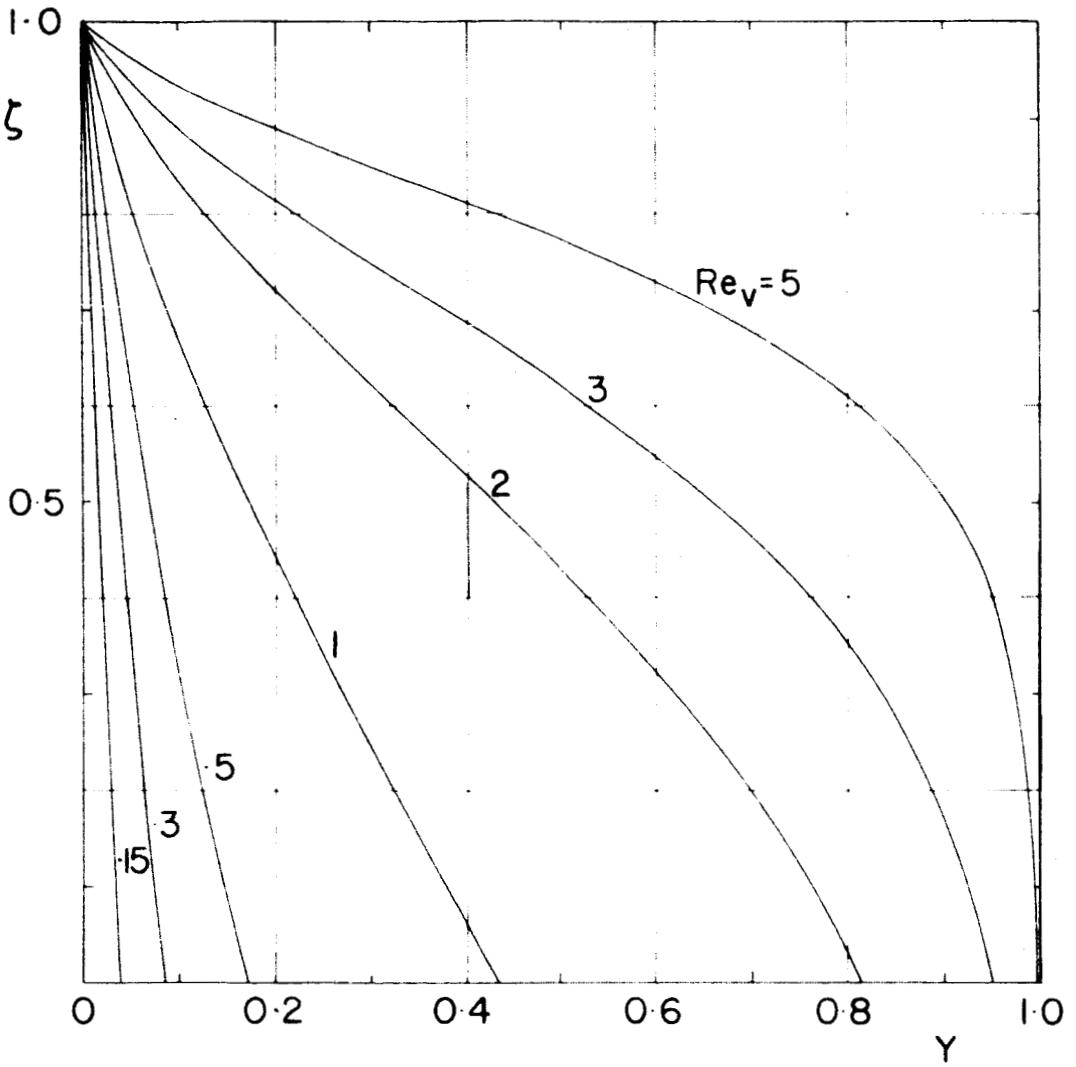

Hydrogen Nitrogen

M_e = 12 T_w = 872°K

Fig. 6

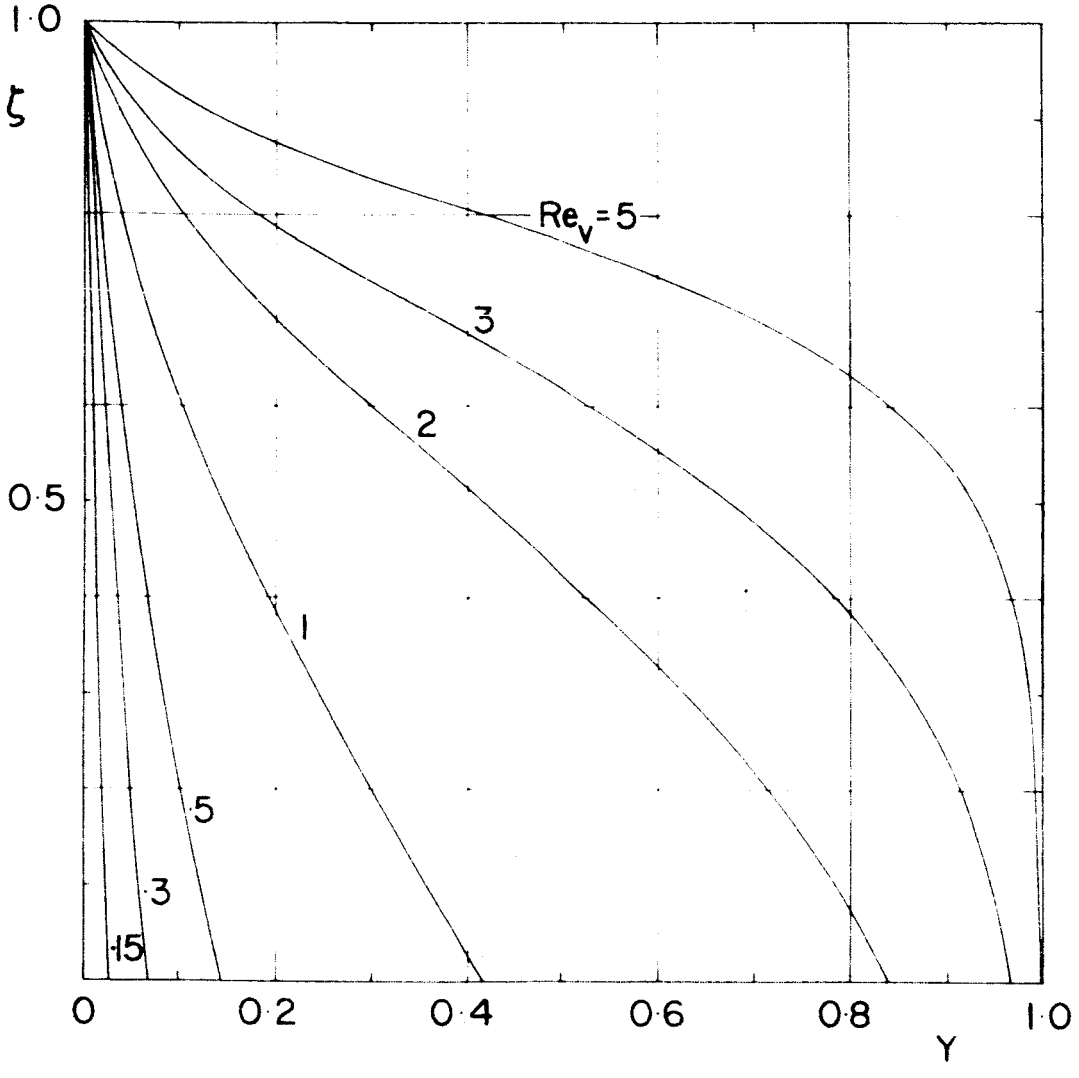

Hydrogen Carbon-dioxide

$M_e = 4$ $T_w = 436°K$

Fig. 7

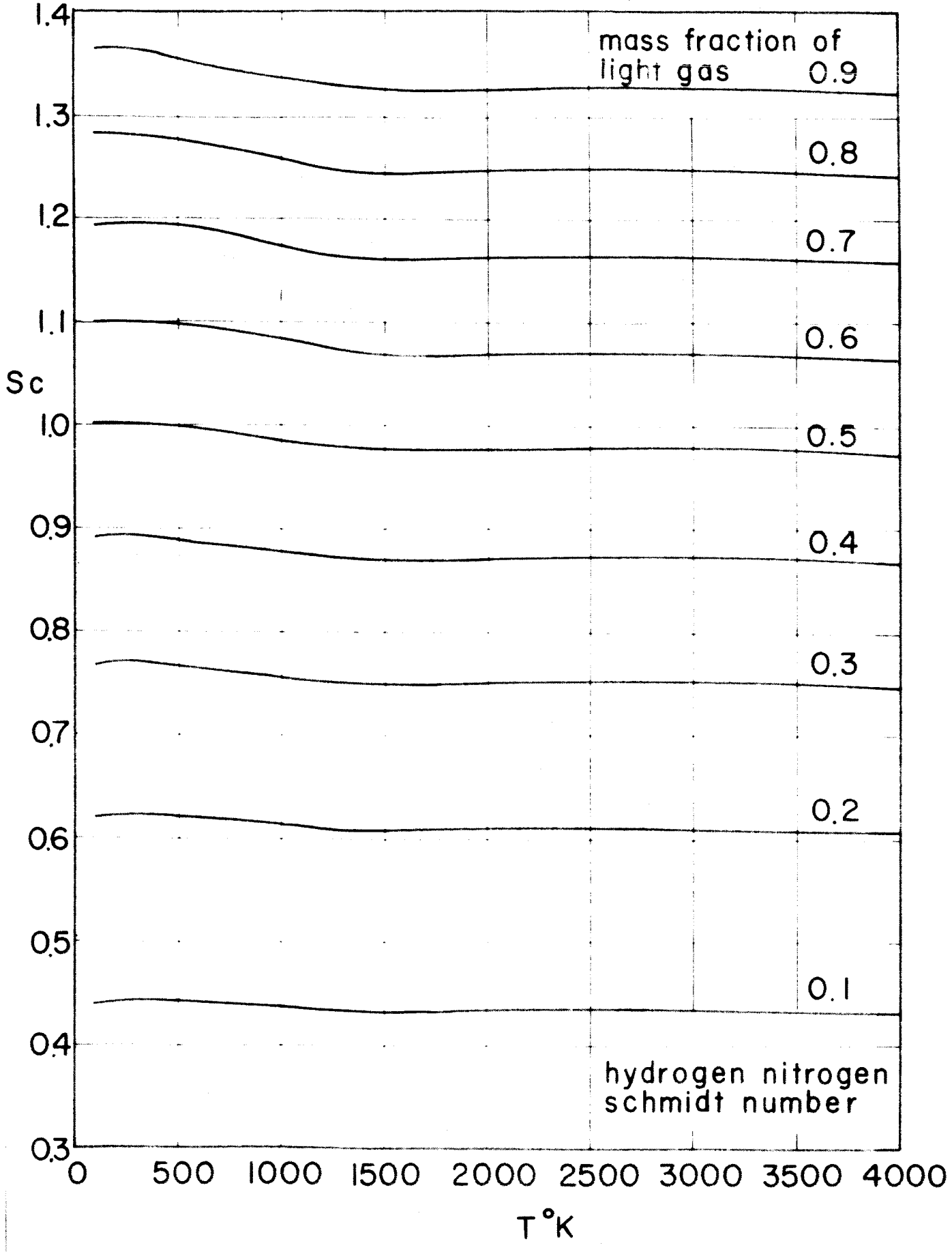
mass fraction of light gas
0.9
0.8
0.7
0.6
0.5
0.4
0.3
0.2
0.1
hydrogen nitrogen schmidt number
Sc
T°K
1.4
1.3
1.2
1.1
1.0
0.9
0.8
0.7
0.6
0.5
0.4
0.3
0
500
1000
1500
2000
2500
3000
3500
4000

Fig. 8

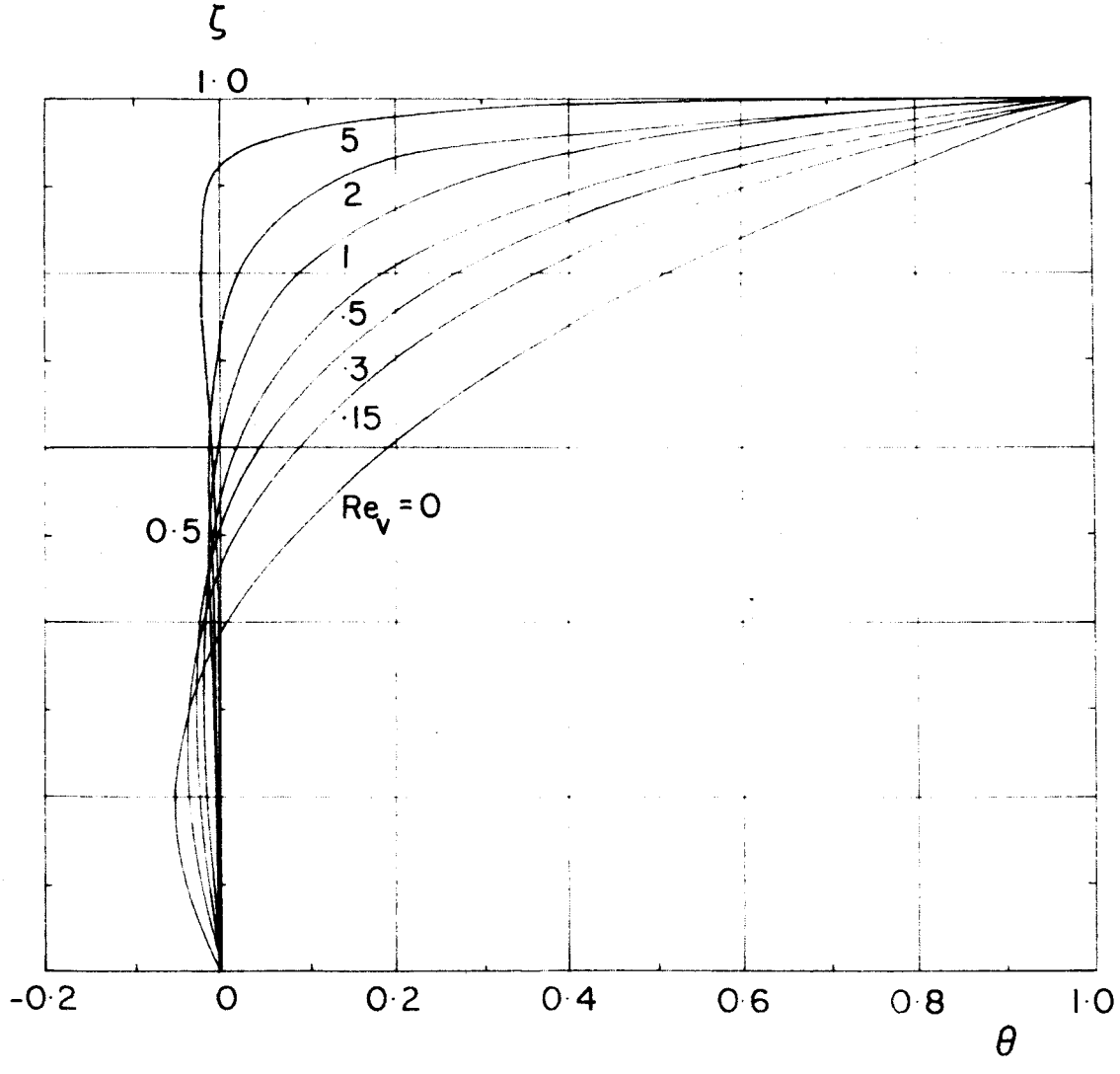

Hydrogen Carbon-dioxide Mixture

$M_e = 4$ $T_w = 436°K$

Fig. 9

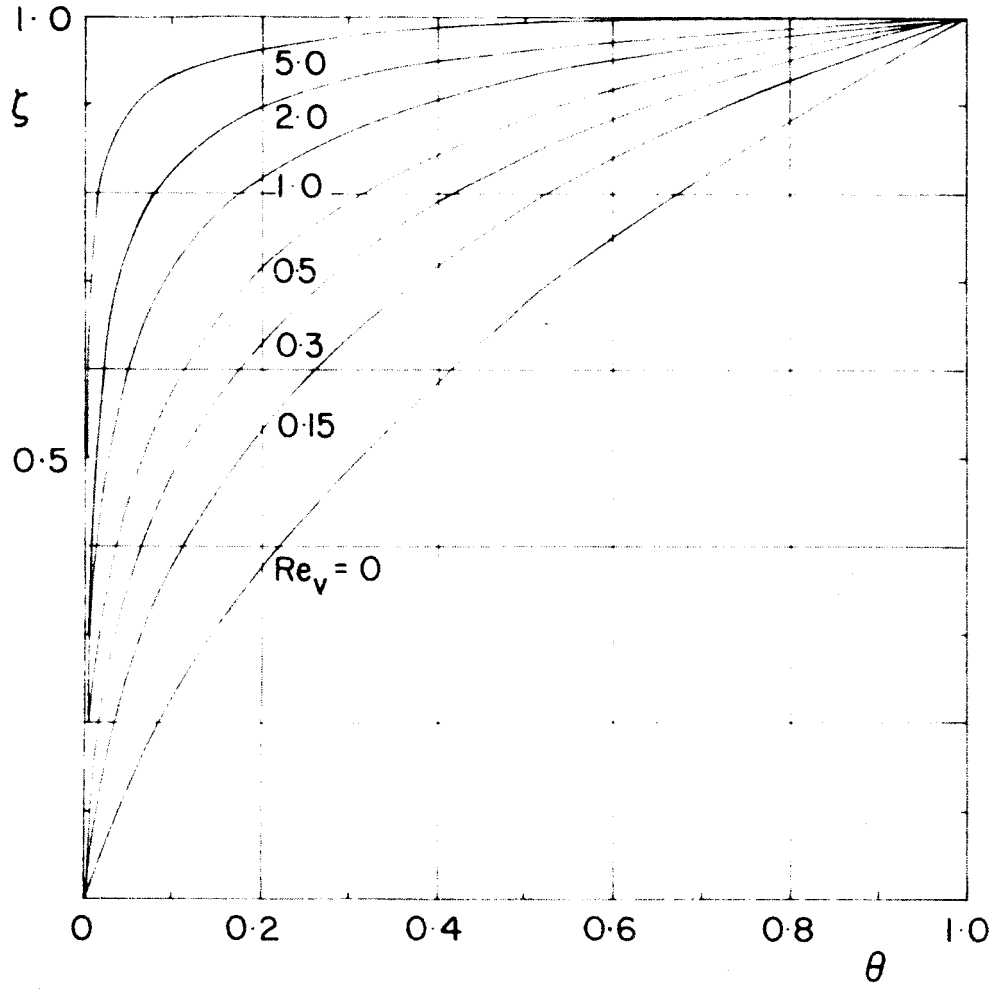

Hydrogen Nitrogen Mixture

Me = 4 Tw = 872 °K

Fig. 10

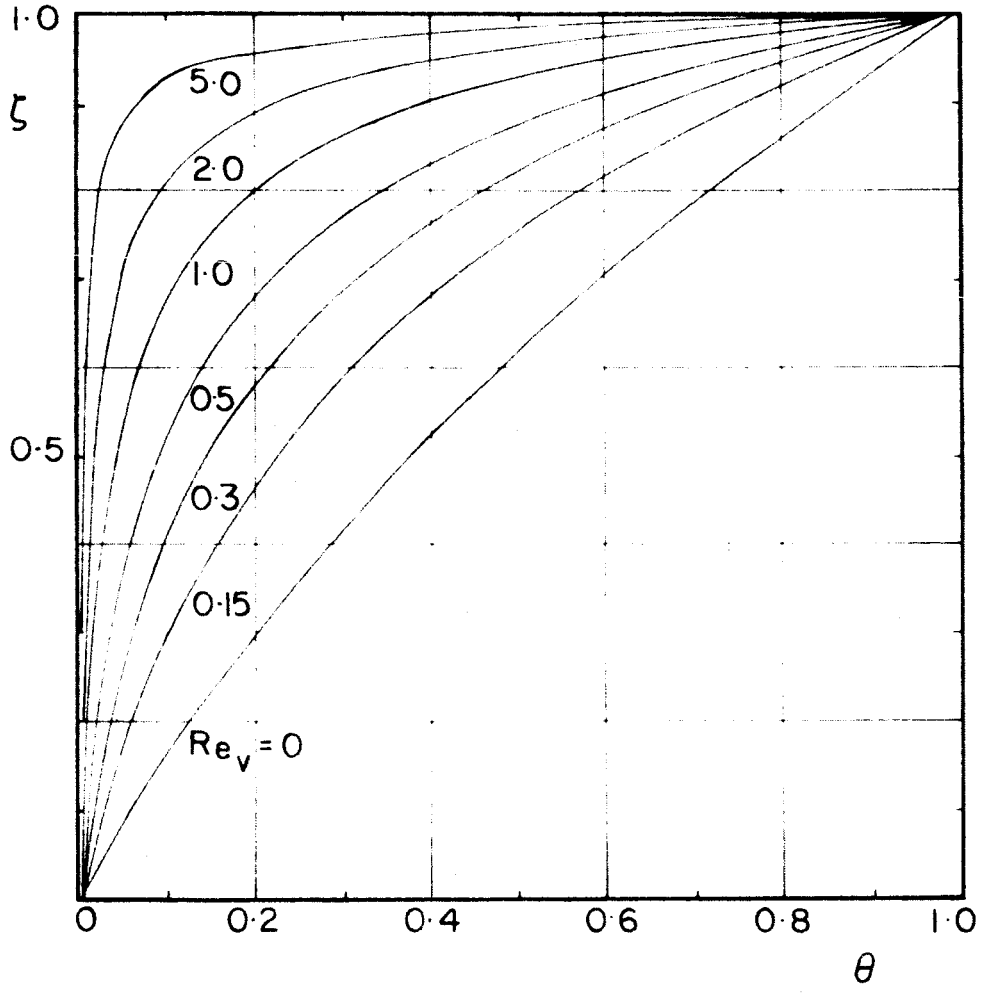

Hydrogen Nitrogen Mixture

Me = 4 Tw = 1308° K

Fig. 11

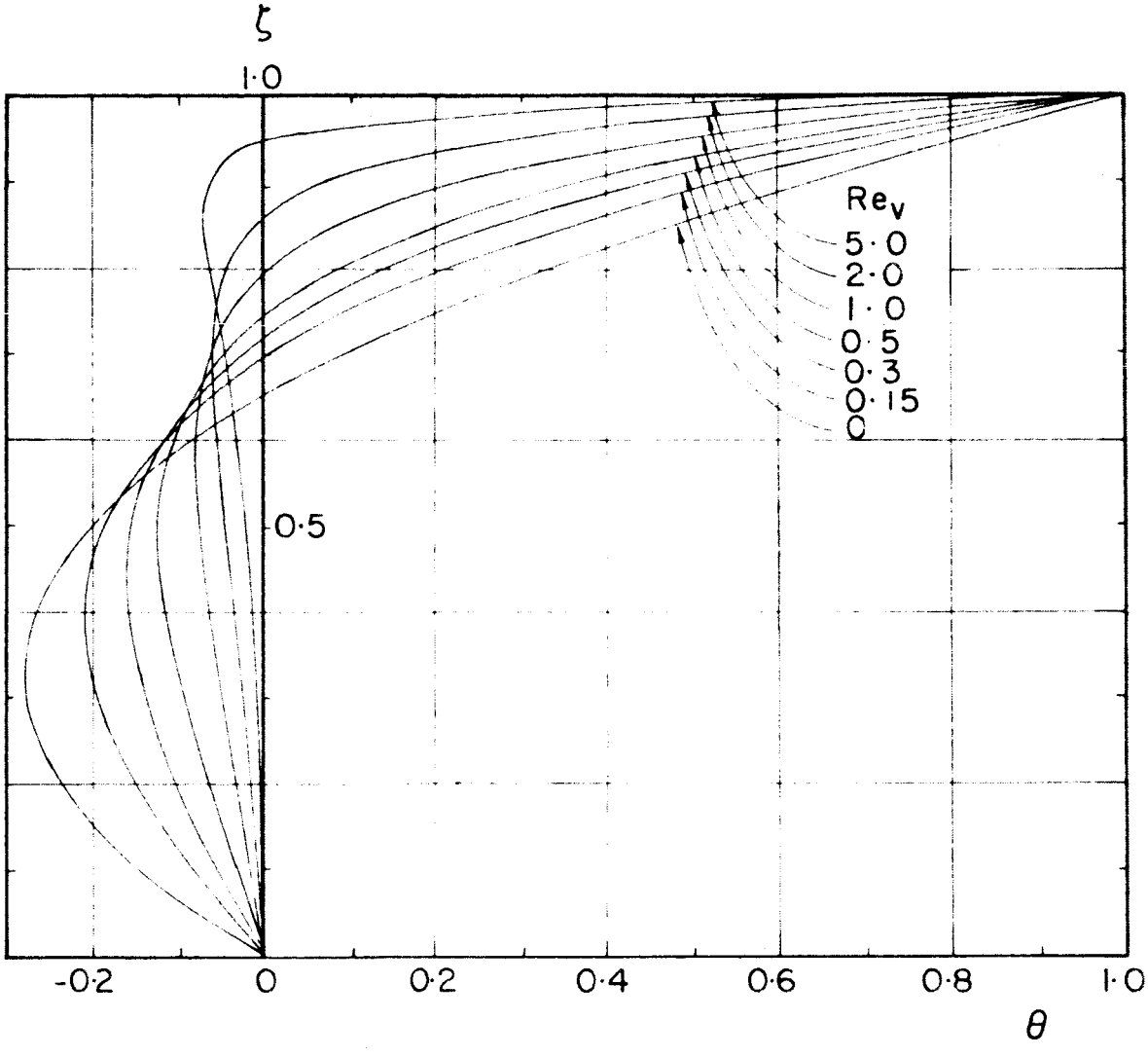

Hydrogen Nitrogen Mixture

Me = 8 Tw = 872 °K

Fig. 12

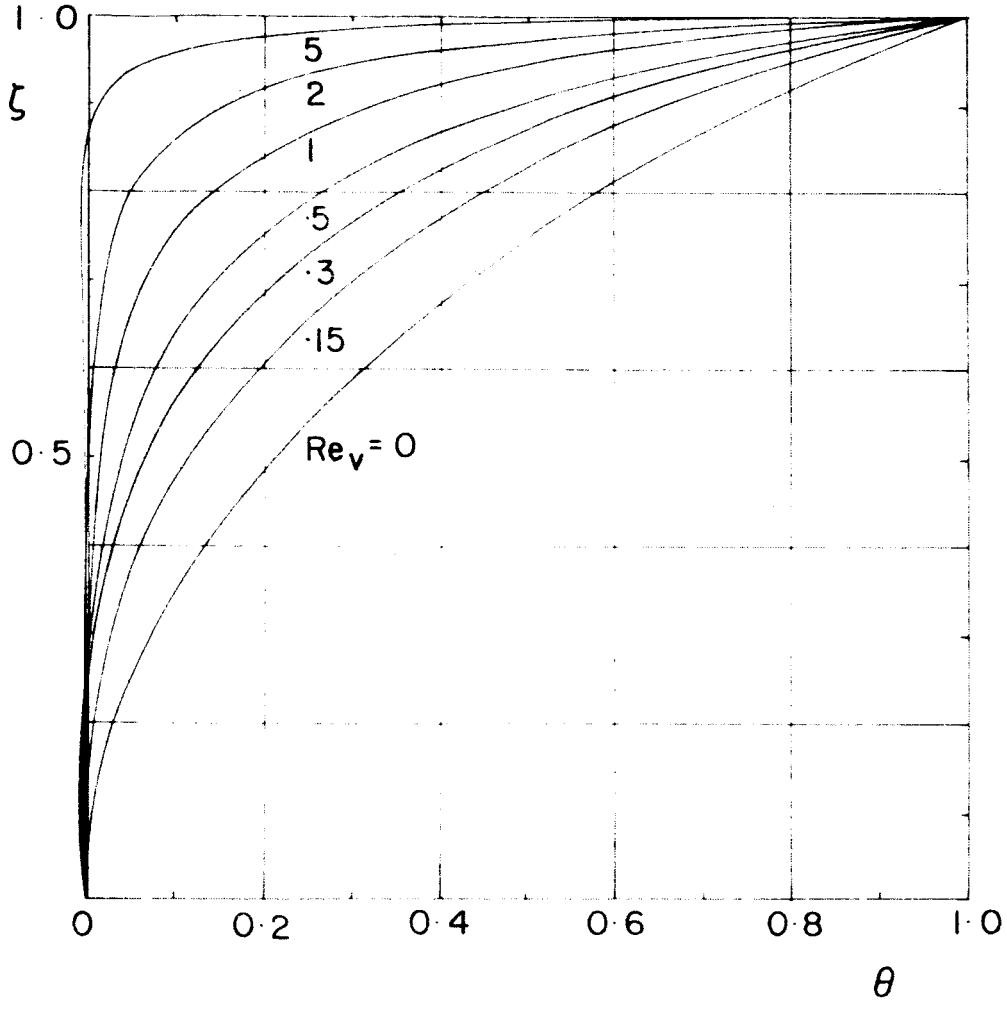

Hydrogen Carbon-dioxide Mixture

$M_e = 8$ $T_w = 1308°K$

Fig. 13

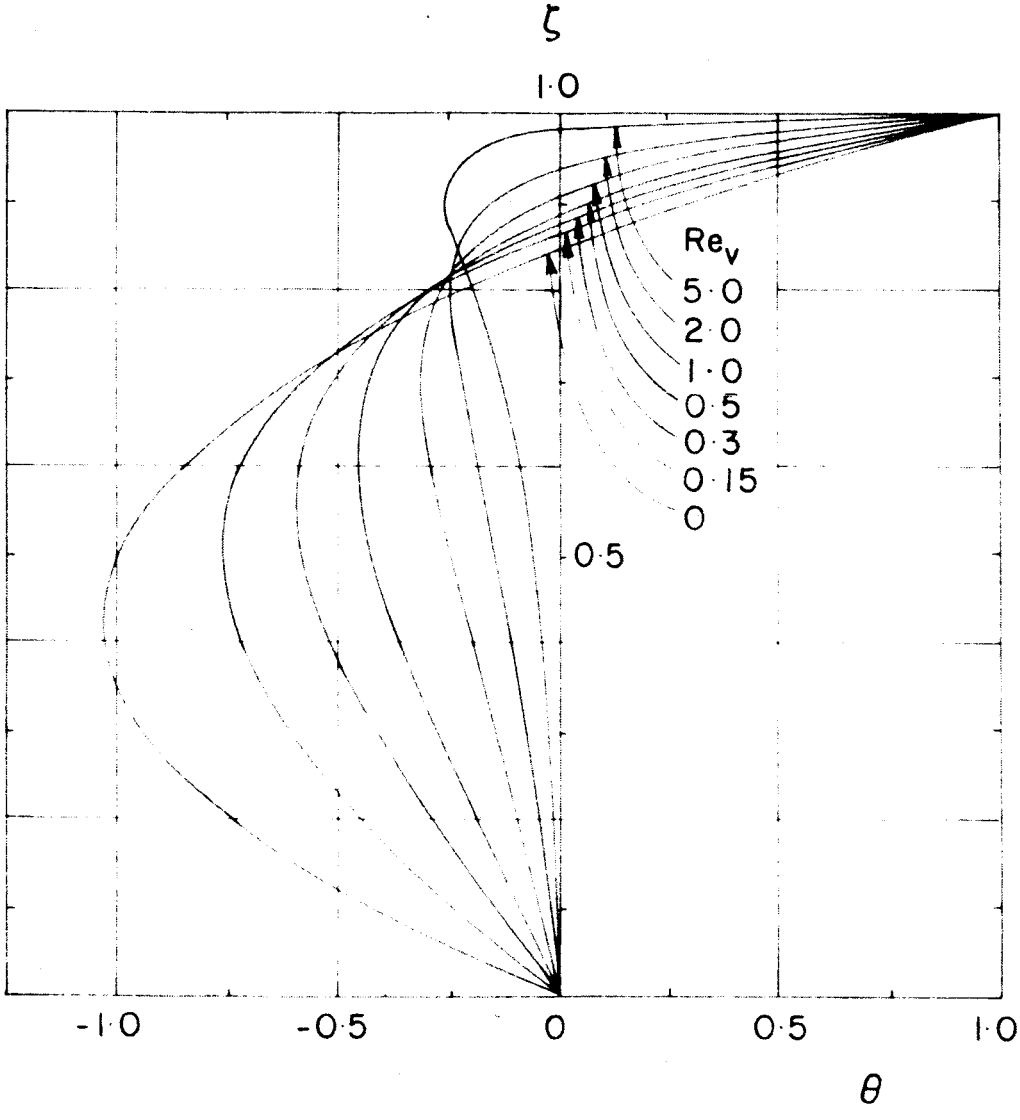

Hydrogen Nitrogen Mixture

Me = 12 Tw = 872 °K

Fig. 14

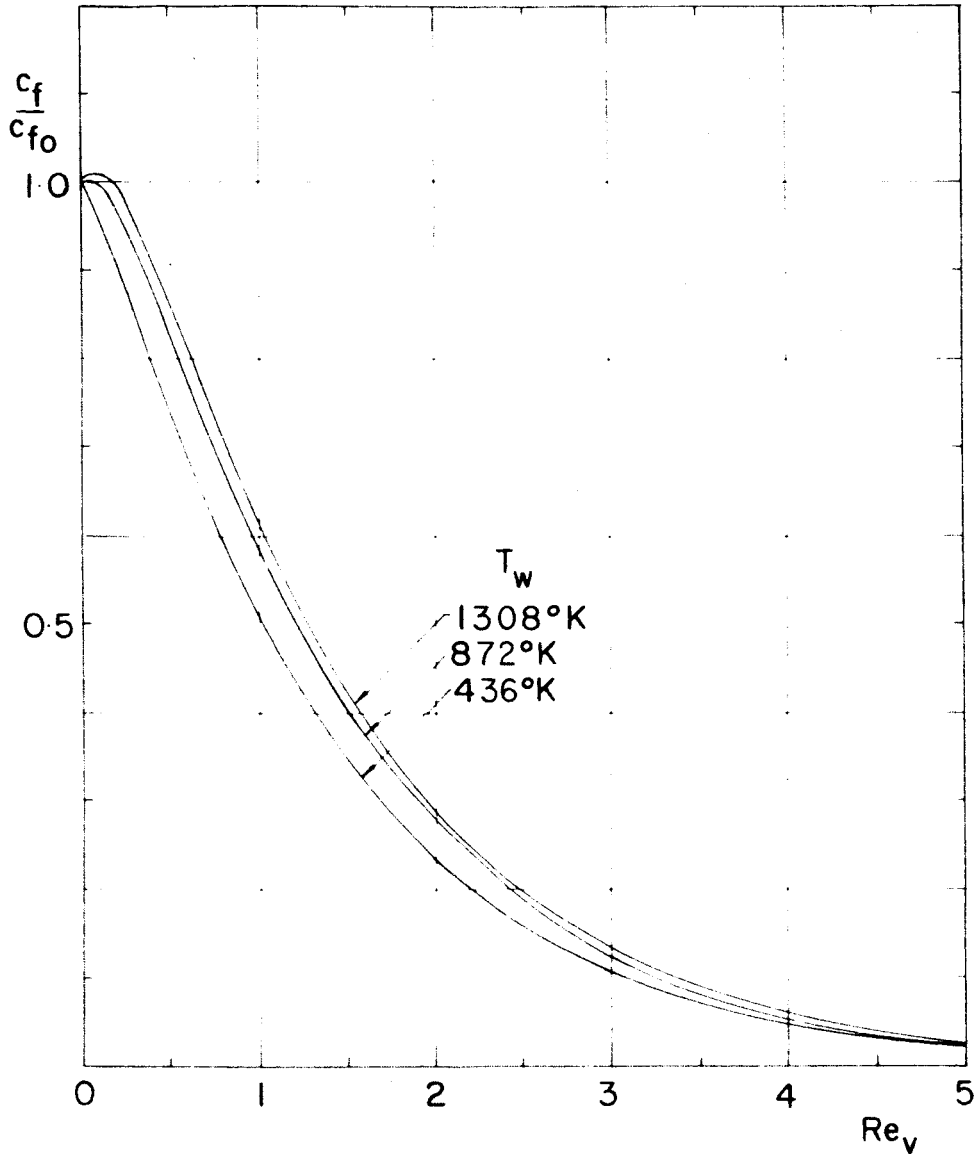

Hydrogen Nitrogen
$M_e = 4$ $T_e = 218°K$

Fig. 15

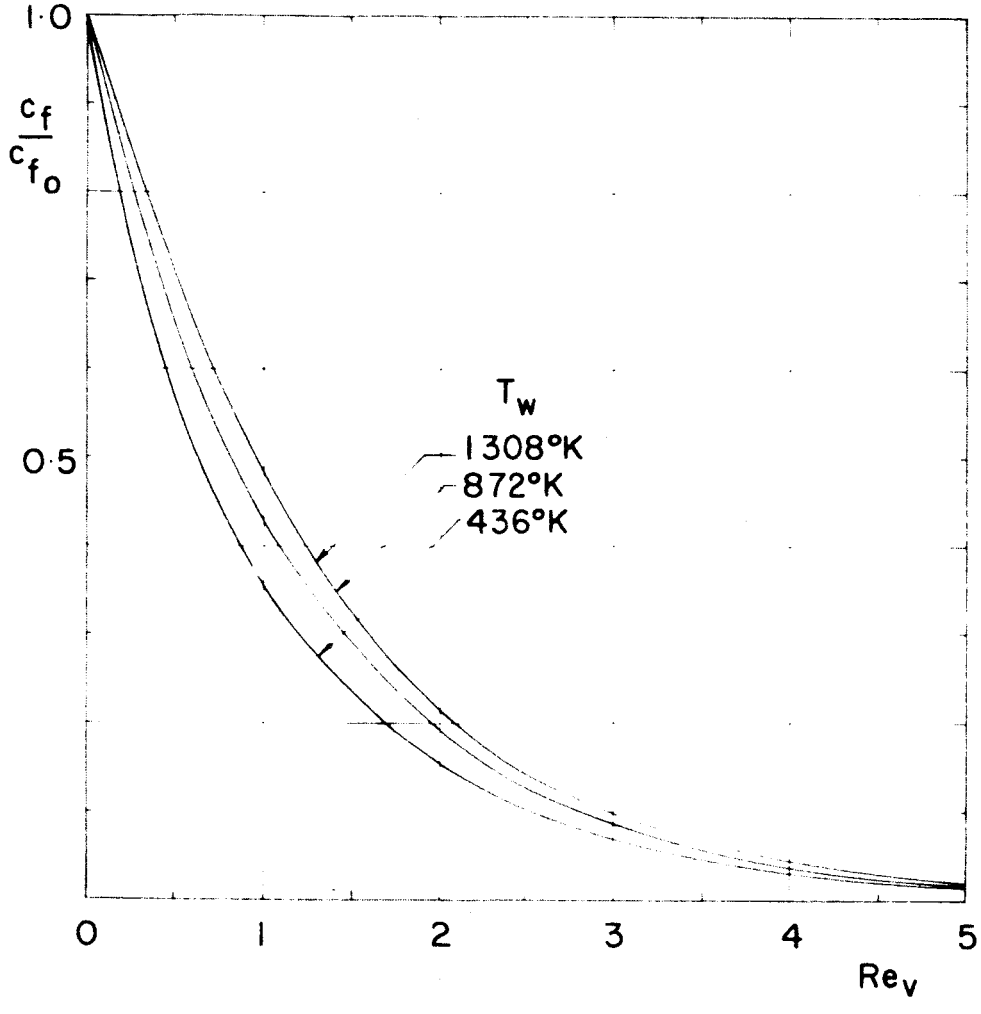

Hydrogen Nitrogen

$M_e = 12$ $T_e = 218°K$

Fig. 16

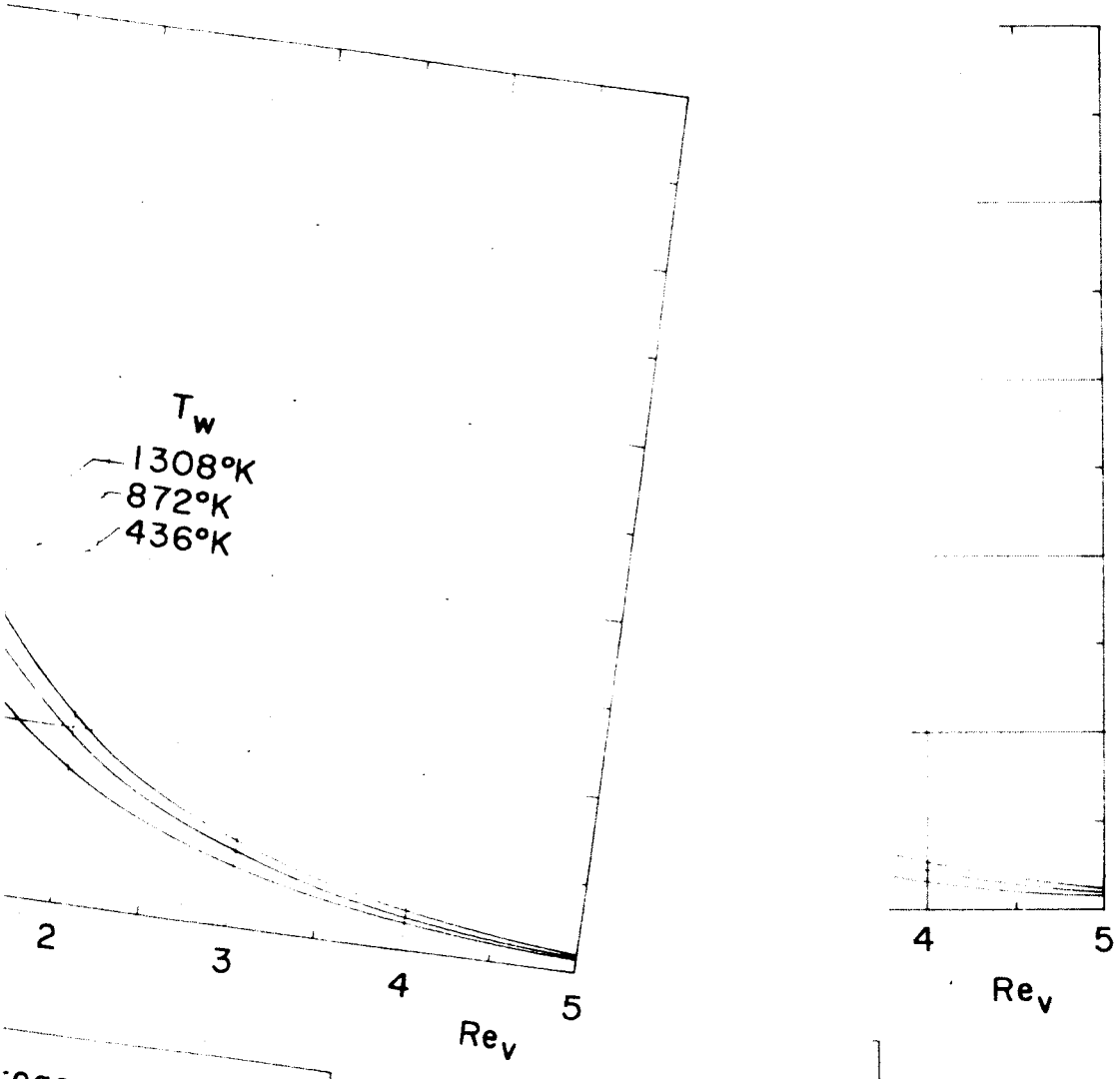

·ogen Nitrogen
12 T_e = 218°K

FIG. 16

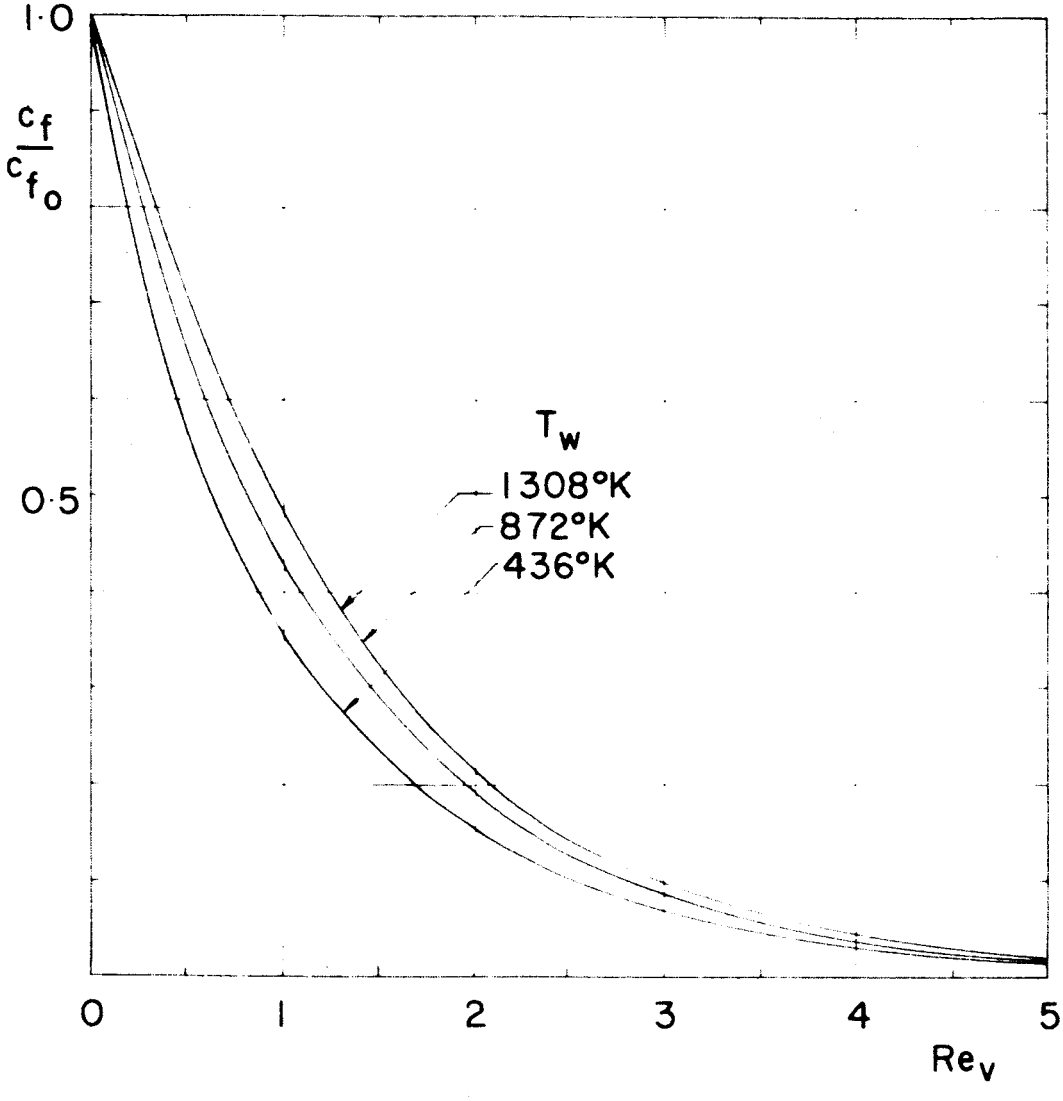

Hydrogen Nitrogen

$M_e = 12$ $T_e = 218°K$

Fig. 16

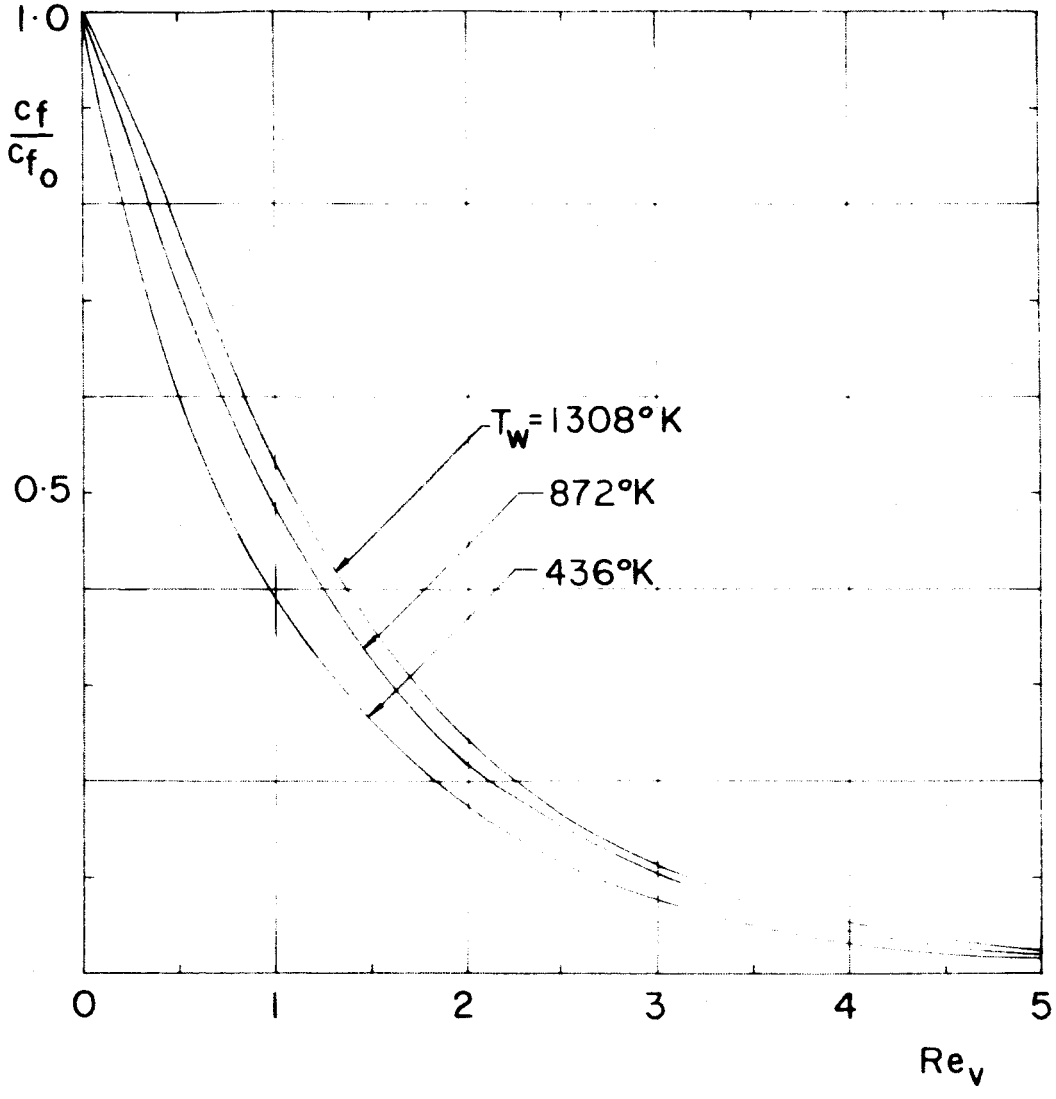

Hydrogen Carbon-dioxide
Mixture M_e = 12

Fig. 17

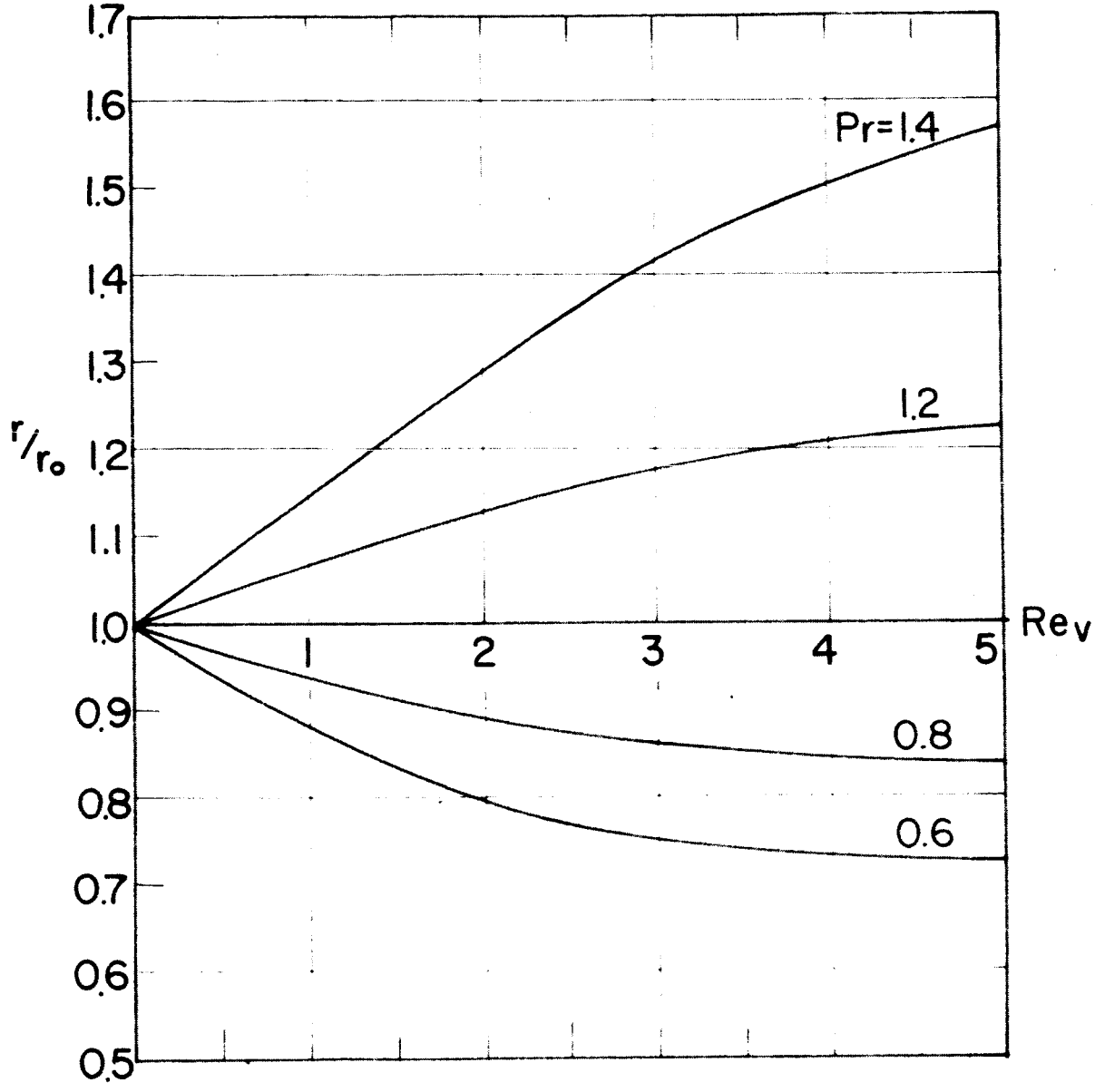

Fig. 13

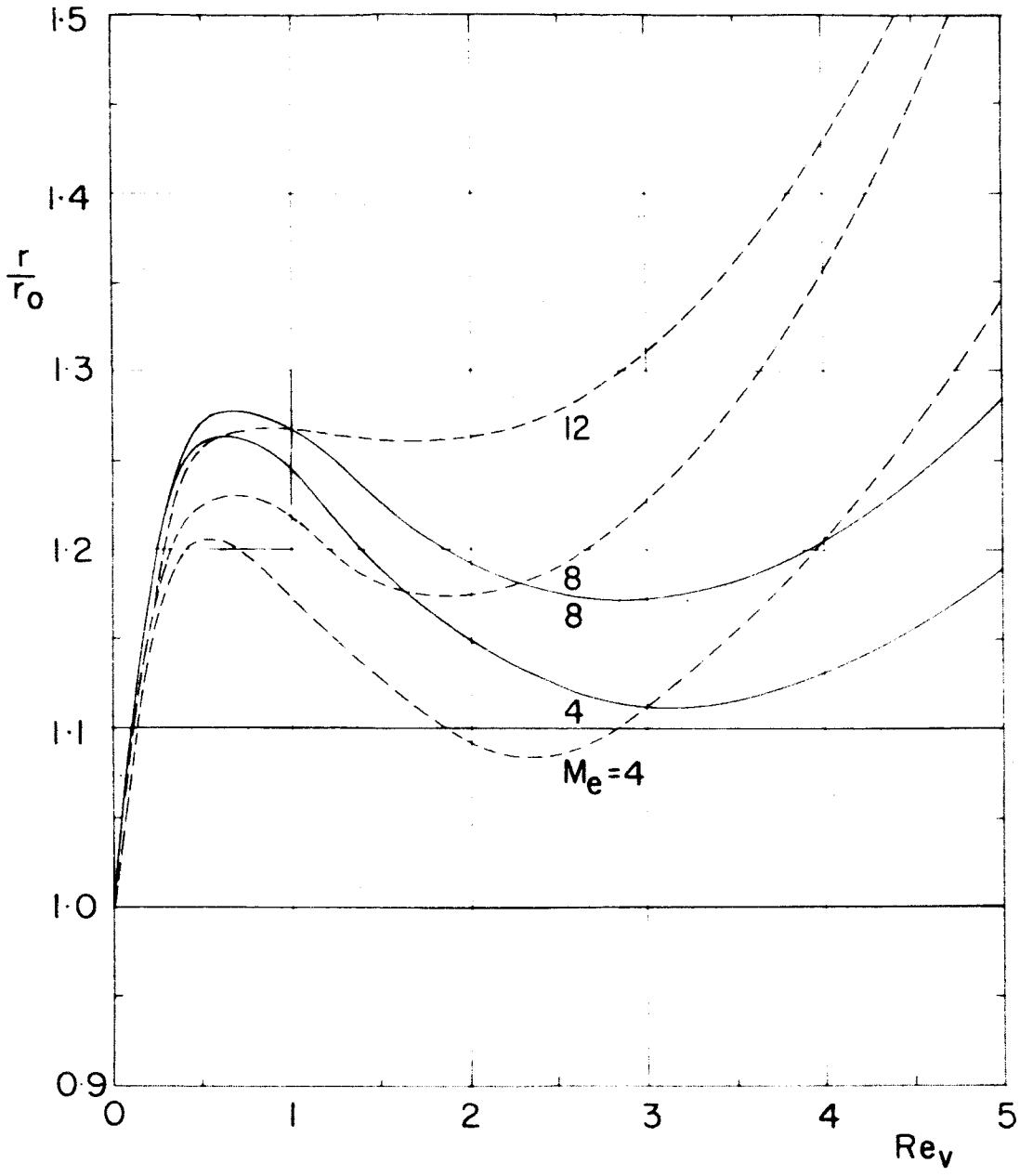
1·5
1·4
r/r0
1·3
1·2
1·1
1·0
0·9
0
1
2
3
4
5
Rev
12
8
8
4
Me=4
Recovery Factor Ratio
H2 : N2
H2 : CO2

Fig. 19

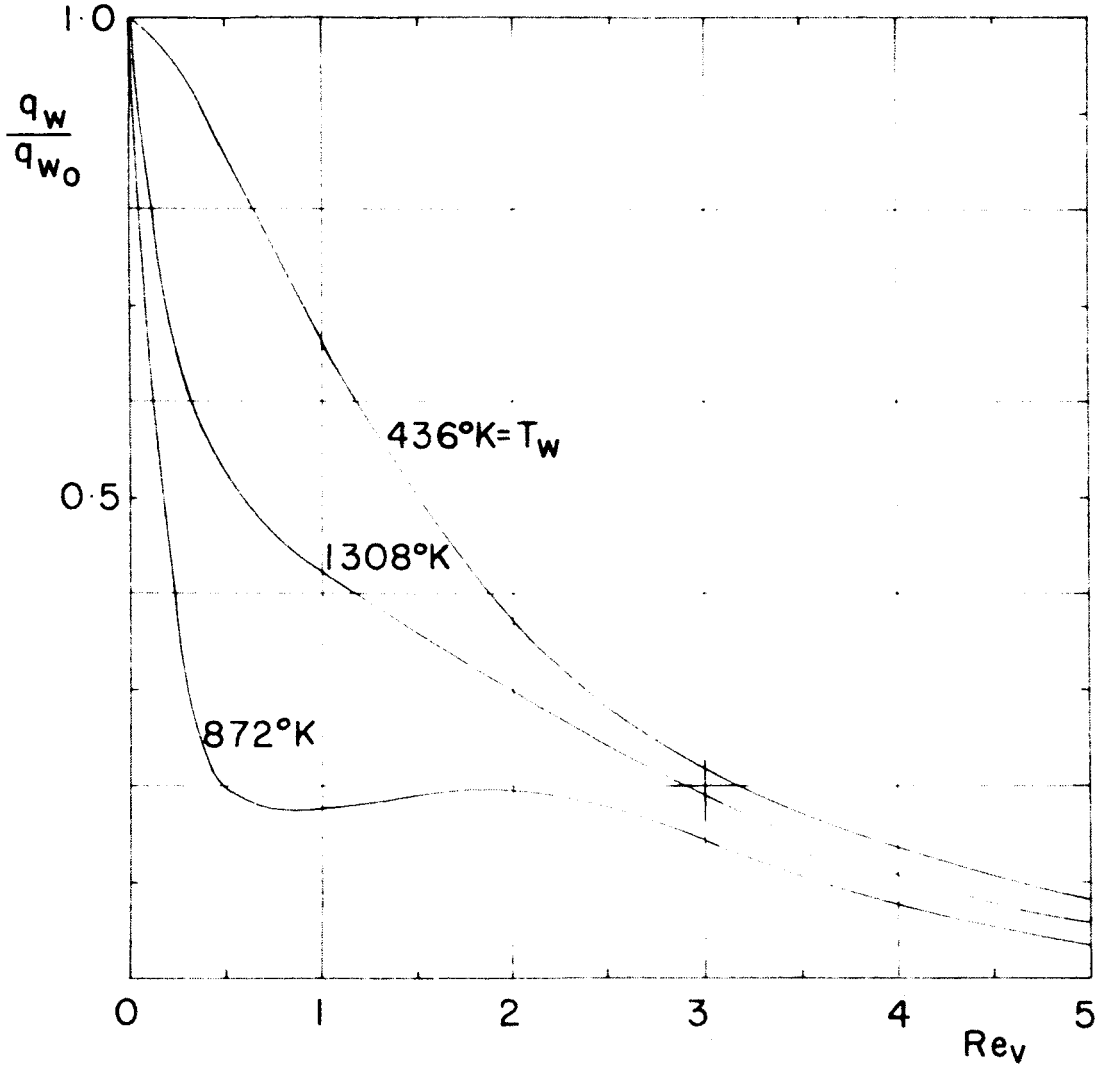

Hydrogen Nitrogen

$M_e = 4$ $T_e = 218°K$

Fig. 20

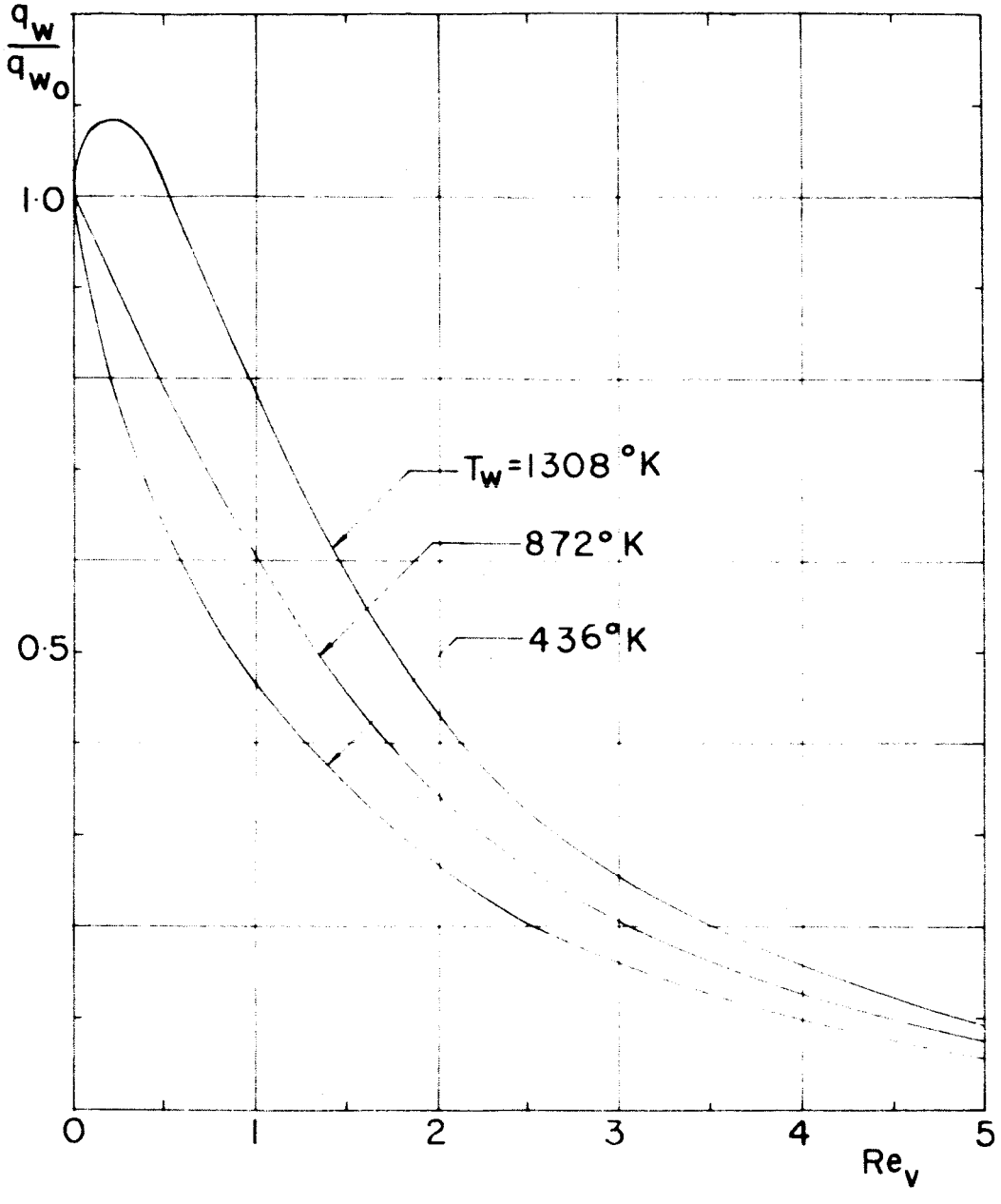

Hydrogen Nitrogen

M_e= 8 T_e= 218 °K

Fig. 21

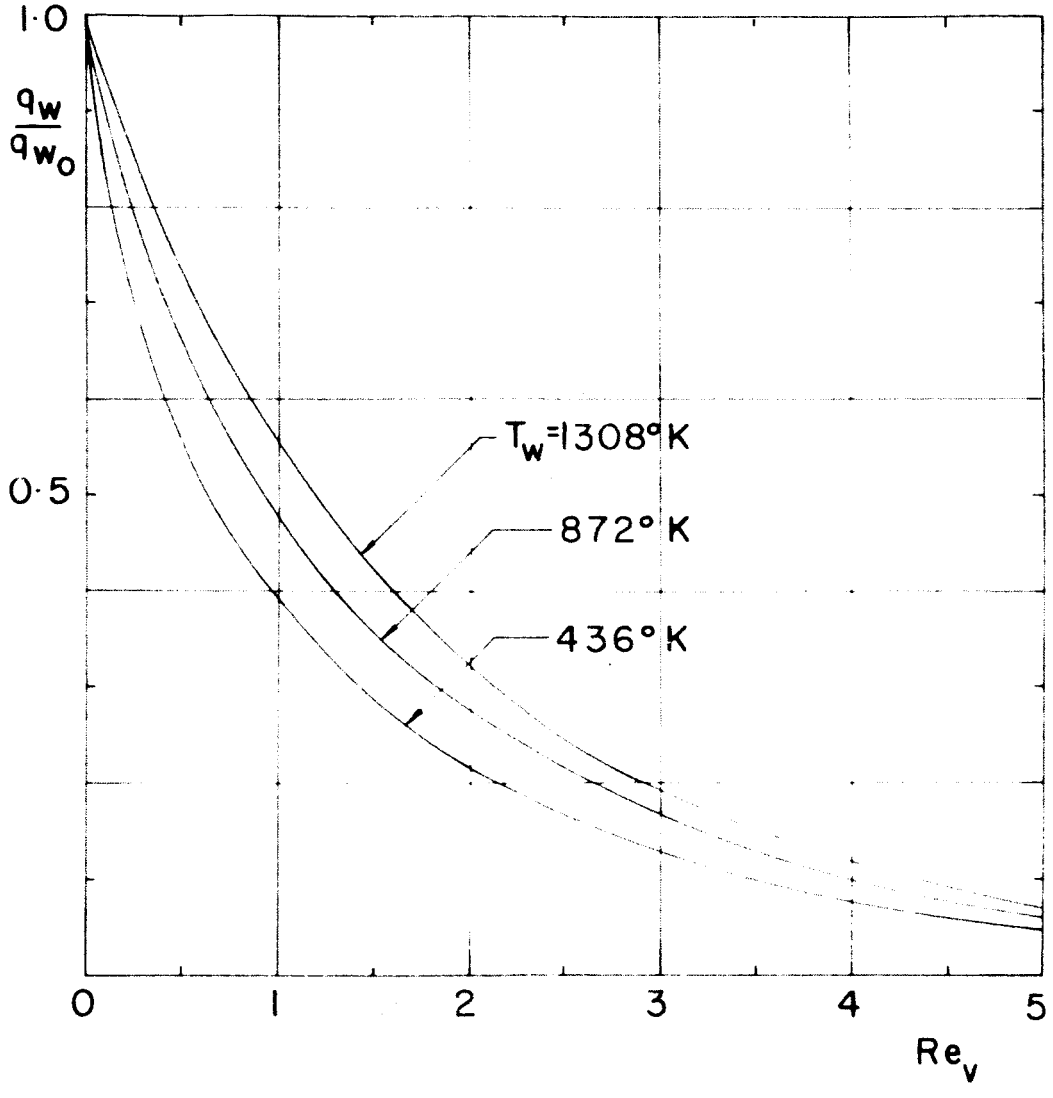

Hydrogen Nitrogen
M_e=12 T_e=218°K

Fig. 22

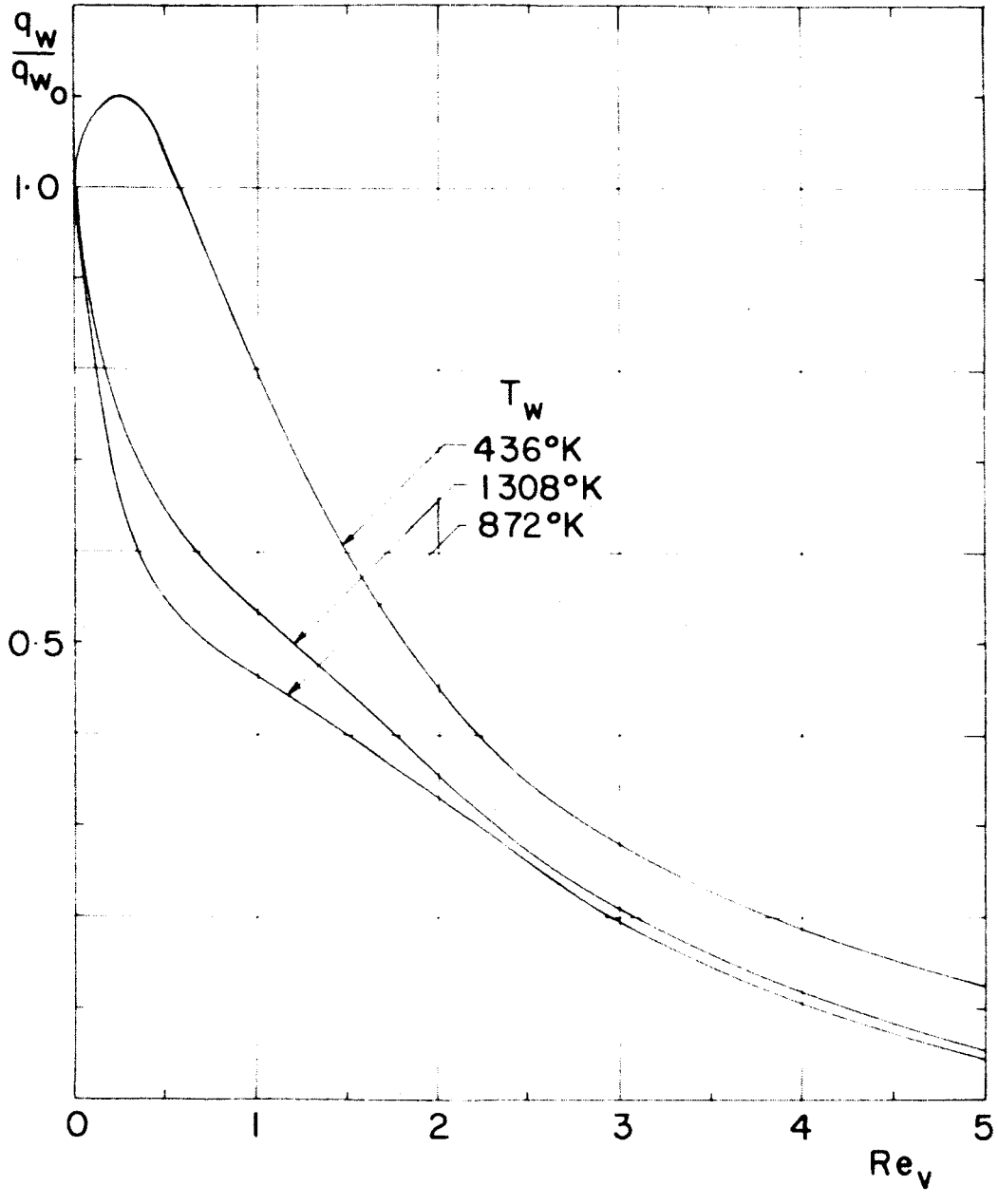

Hydrogen Carbon-dioxide

$M_e = 4$ $T_e = 218°K$

Fig. 23

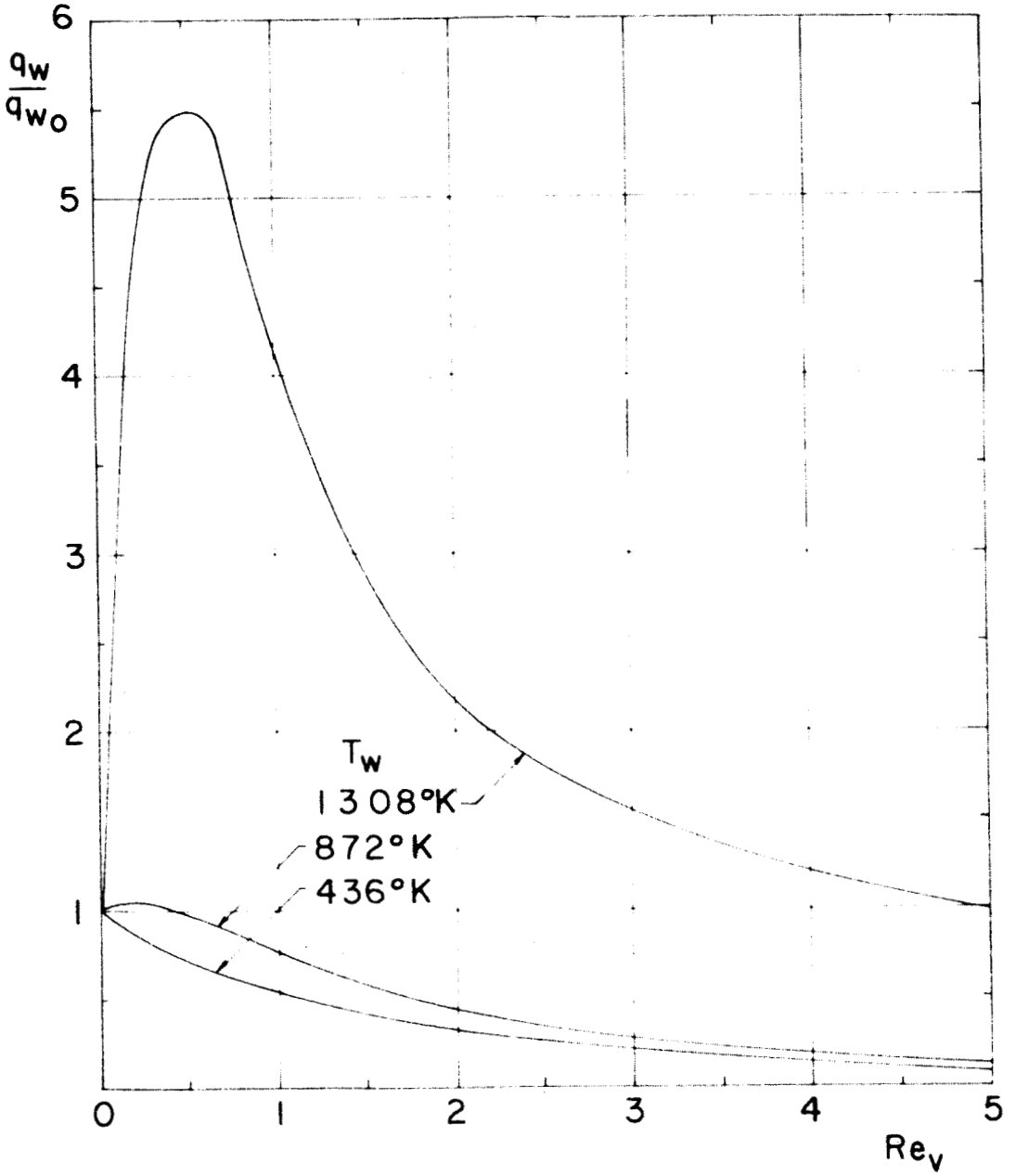

Hydrogen Carbon-dioxide

$M_e = 8$ $T_e = 218°K$

Fig. 24

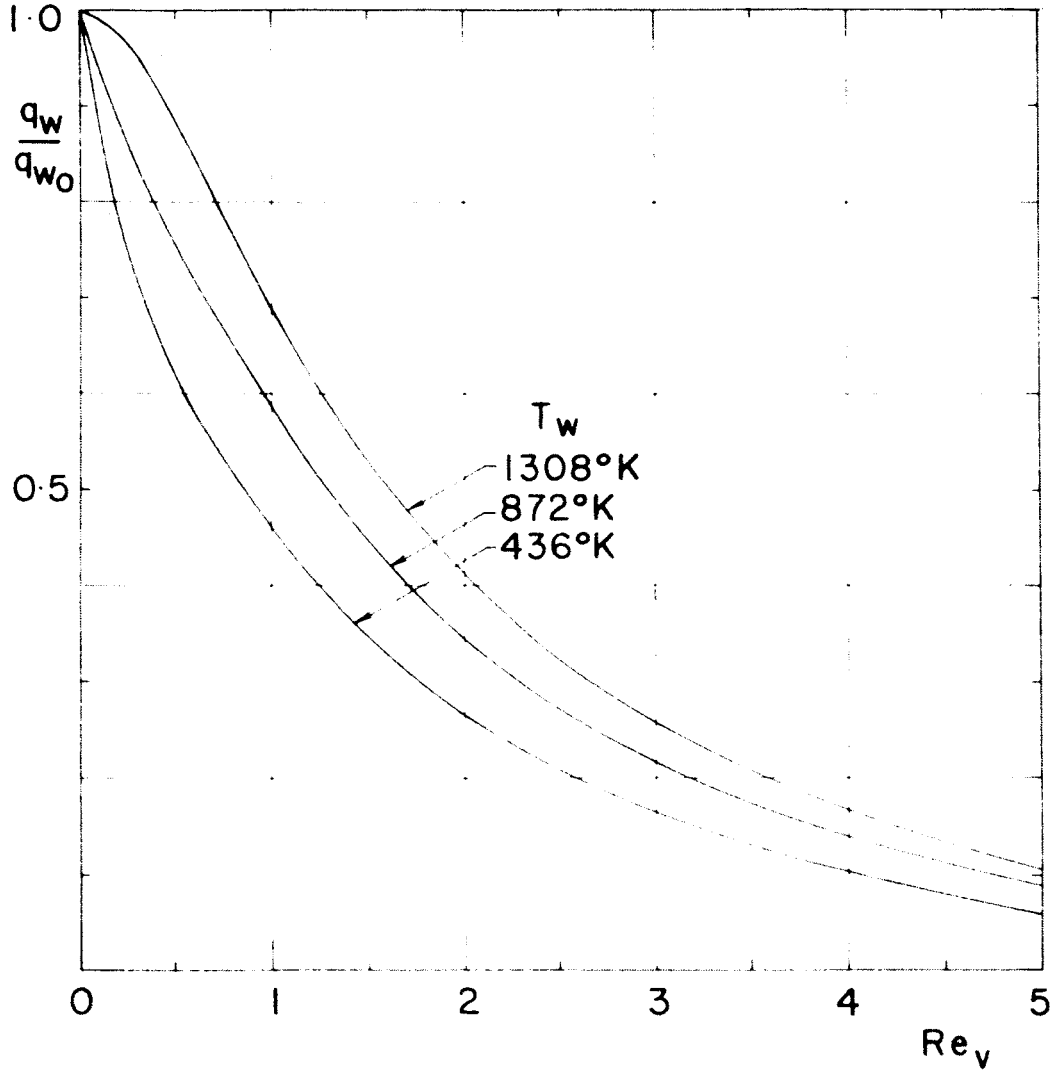

Hydrogen Carbon-dioxide

$M_e = 12 \quad T_e = 218°K$

Fig. 23

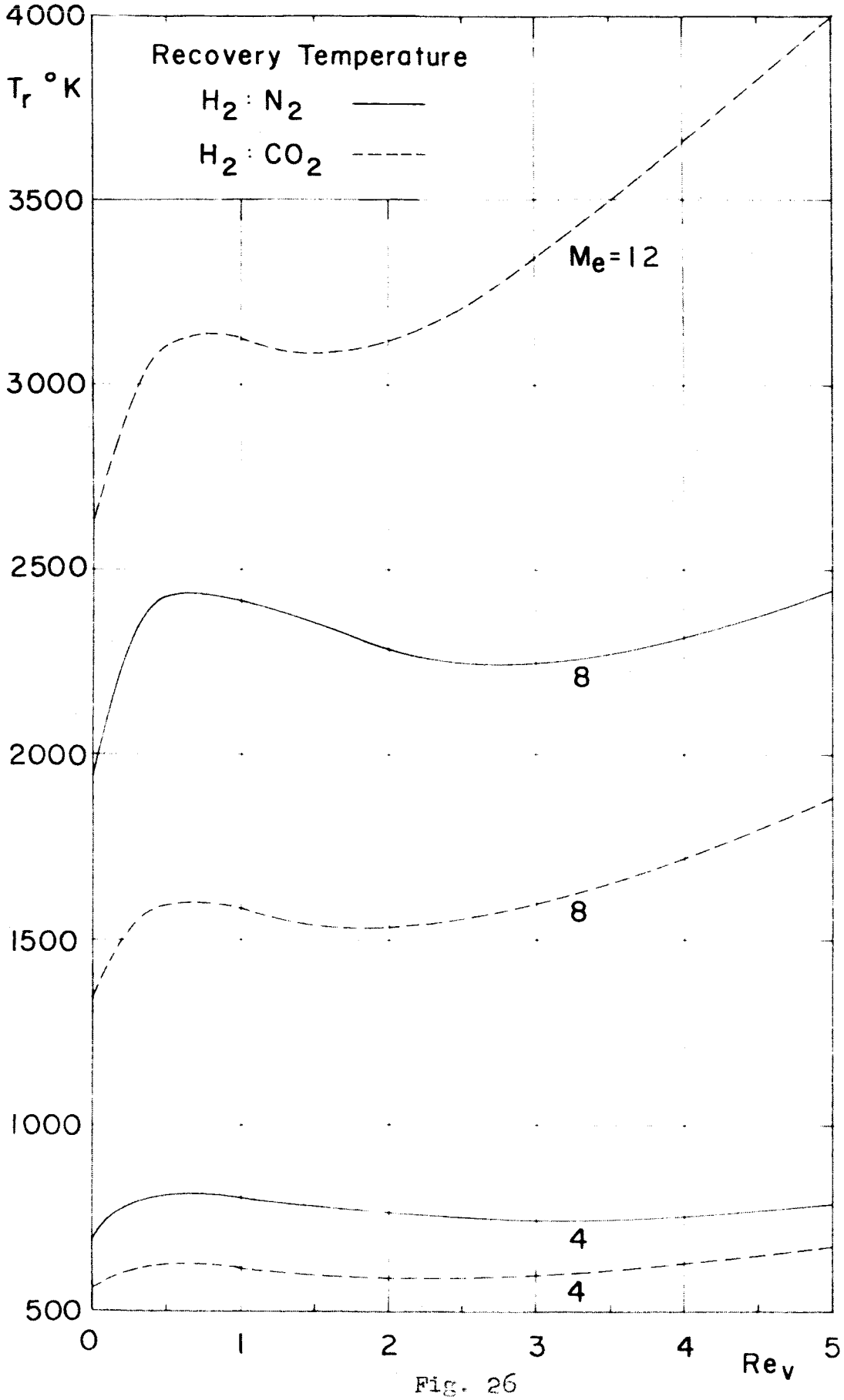
Recovery Temperature
$H_2 : N_2$
$H_2 : CO_2$
T_r °K
4000
3500
3000
2500
2000
1500
1000
500
0
1
2
3
4
5
Re_v
$M_e = 12$
8
8
4
4

Fig. 26

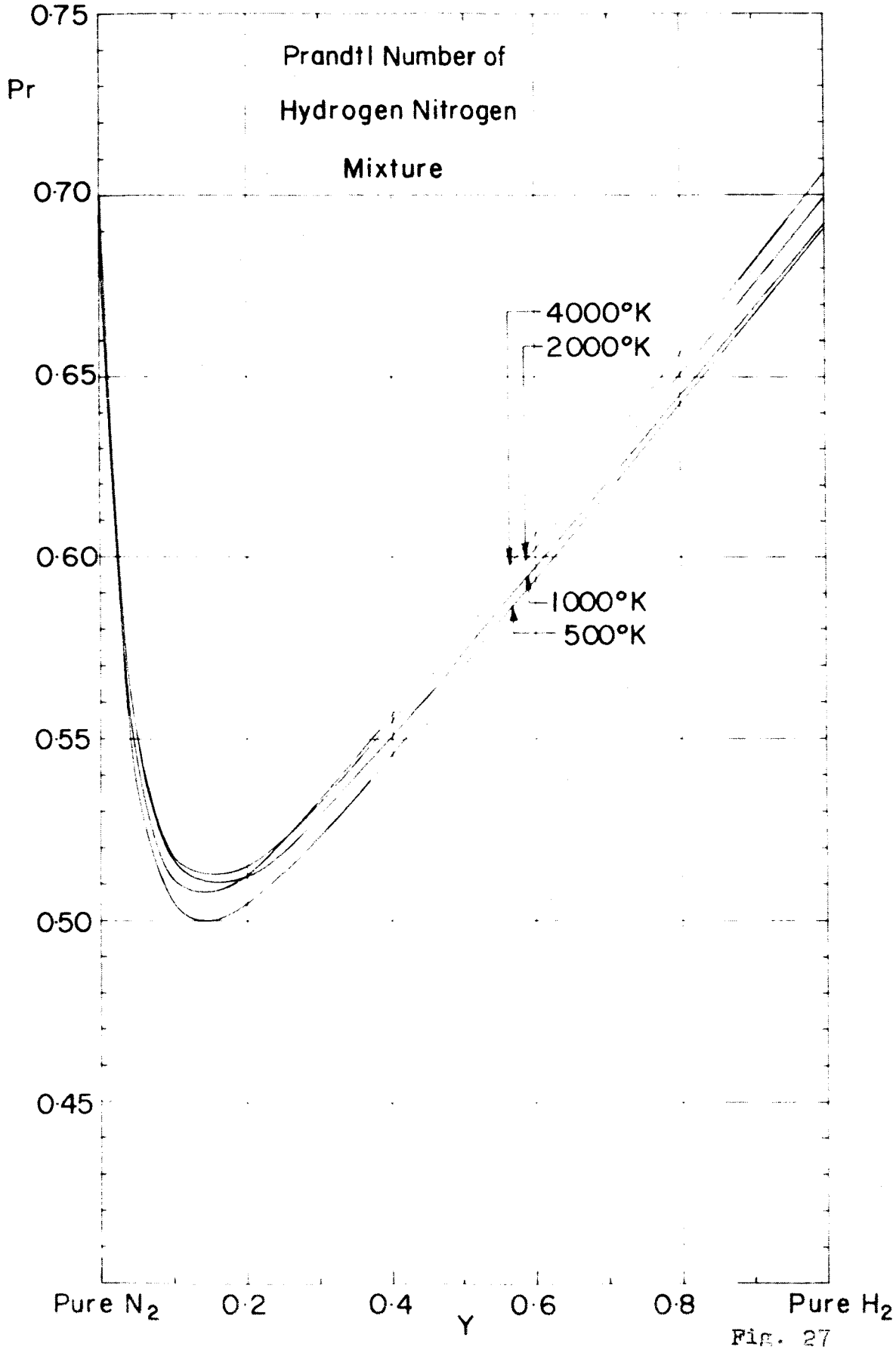
Prandtl Number of
Hydrogen Nitrogen
Mixture
Pr
0·75
0·70
0·65
0·60
0·55
0·50
0·45
4000°K
2000°K
1000°K
500°K
Pure N2
0·2
0·4
0·6
0·8
Pure H2
Y

Fig. 27

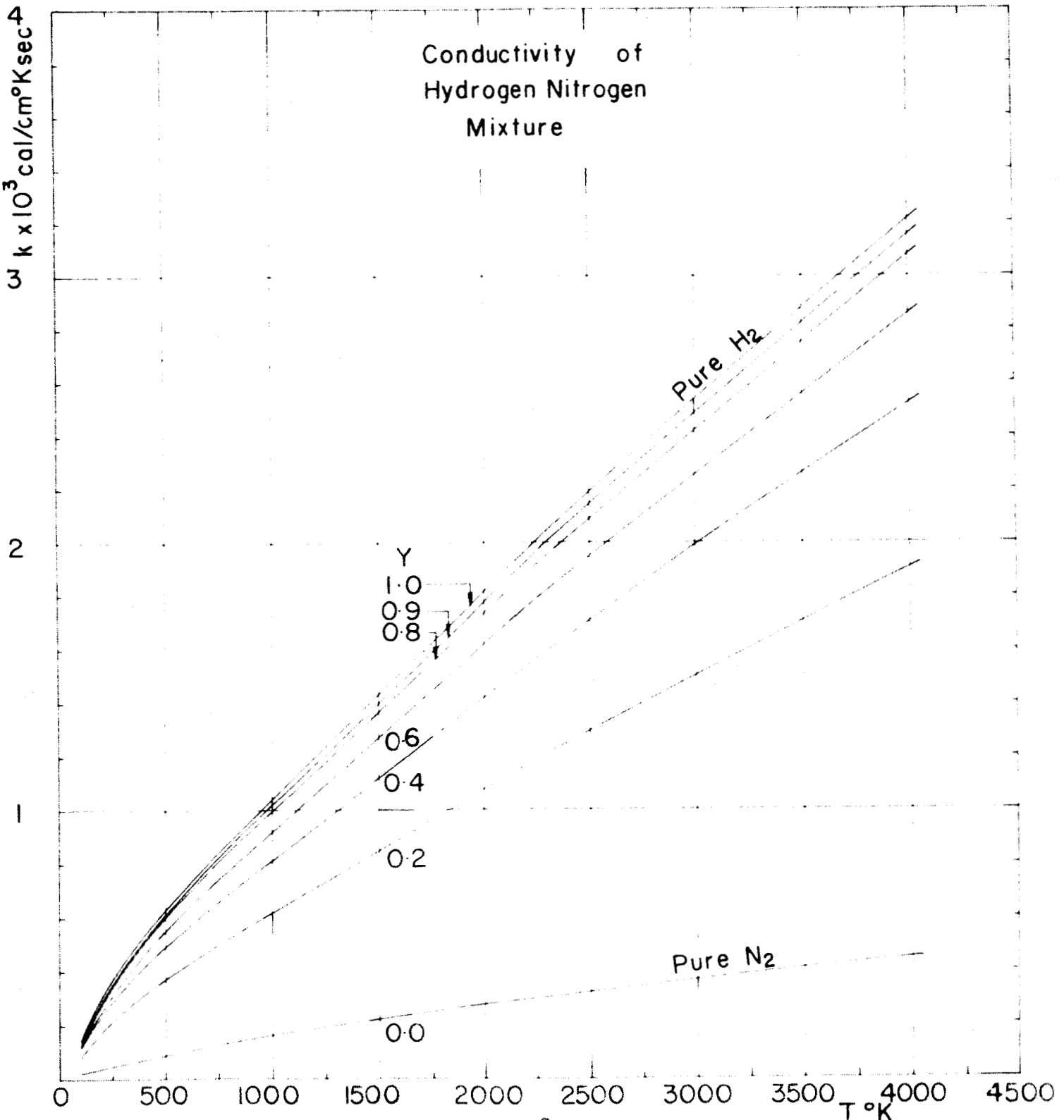
Conductivity of
Hydrogen Nitrogen
Mixture
3 k x 10^3 cal/cm°K sec^4
2
1
Pure H2
Y
1·0
0·9
0·8
0·6
0·4
0·2
Pure N2
0·0
0
500
1000
1500
2000
2500
3000
3500
4000
4500
T °K

Fig. 28

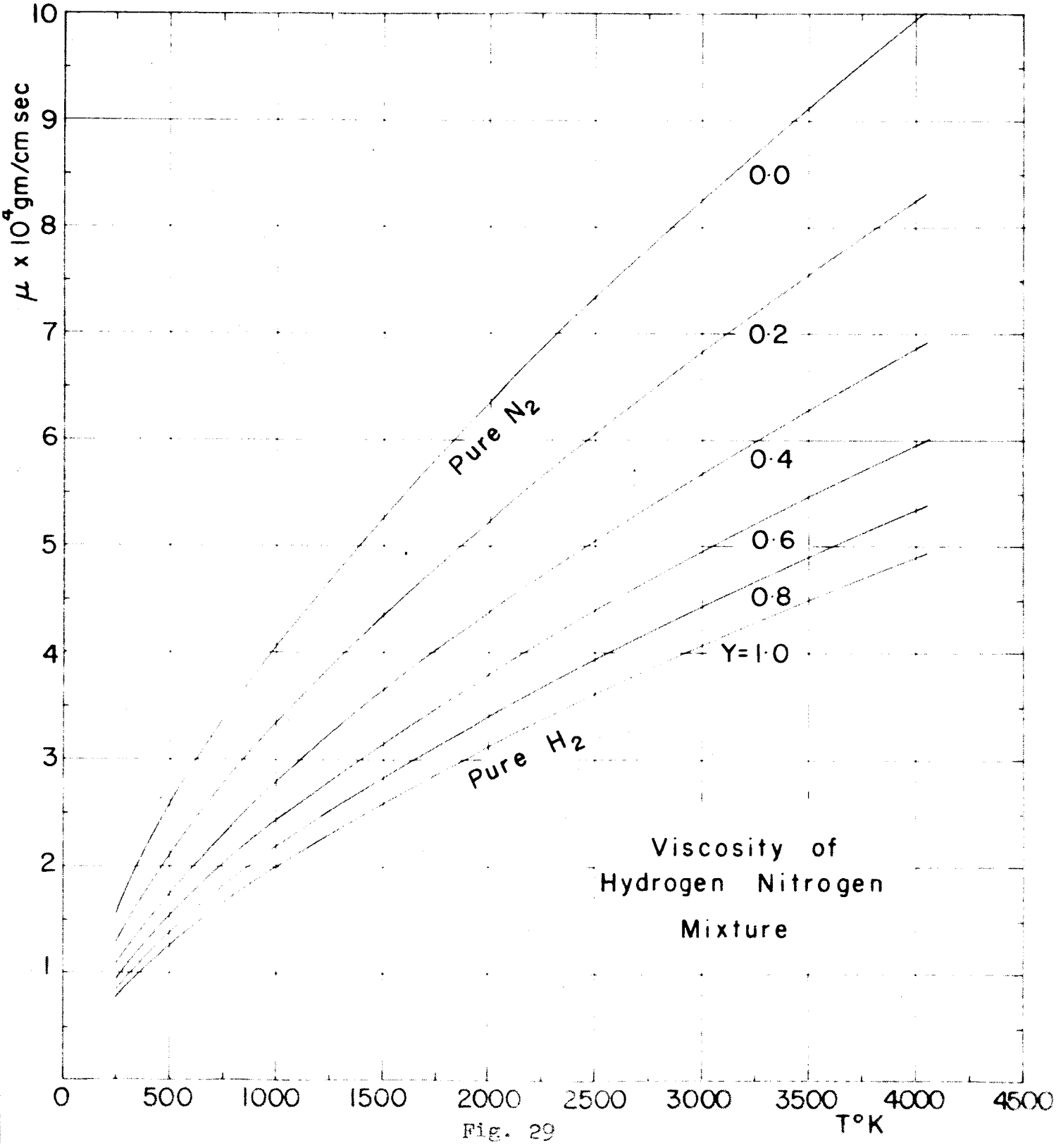
10
9
8
7
6
5
4
3
2
1
μ x 10⁴ gm/cm sec
0·0
0·2
0·4
0·6
0·8
Y=1·0
Pure N2
Pure H2
Viscosity of
Hydrogen Nitrogen
Mixture
0
500
1000
1500
2000
2500
3000
3500
4000
4500
T°K

Fig. 29